Matrix metalloproteinase-2 ablation in dystrophin-deficient *mdx* muscle reduces angiogenesis resulting in impaired growth of regenerated muscle fibers

Daigo Miyazaki, [1] Akinori Nakamura*, [1] Kazuhiro Fukushima, [1] Kunihiro Yoshida, [1,2] Shin'ichi Takeda, [3] Shu-ichi Ikeda[1]

[1] Department of Medicine (Neurology and Rheumatology), Shinshu University School of Medicine, 3-1-1 Asahi, Matsumoto 390-8621, Japan

[2] Department of Neurogenetics, Division of Brain Disease Research, Shinshu University School of Medicine, 3-1-1 Asahi, Matsumoto 390-8621, Japan

[3] Department of Molecular Therapy, Institute of Neuroscience, National Research Center of Neurology and Pscychiatry, 4-1-1 Ogawa-higashi, 187-8521 Kodaira, Tokyo, Japan

Correspondence to Akinori Nakamura, M.D., Ph.D.

Tel: +81-263-37-2673

Fax: +81-263-37-3427

Email: anakamu@shinshu-u.ac.jp

Abstract

Matrix metalloproteases (MMPs) are a family of endopeptidases classified into subgroups based on substrate preference in normal physiological processes such as embryonic development and tissue remodeling, as well as in various disease processes via degradation of extracellular matrix components. Among the MMPs, MMP-9 and MMP-2 have been reported to be up-regulated in skeletal muscle in the lethal X-linked muscle disorder Duchenne muscular dystrophy (DMD), which is caused by loss of dystrophin. A recent study showed that deletion of the *MMP9* gene in *mdx*, a mouse model for DMD, improved skeletal muscle pathology and function; however, the role of MMP-2 in dystrophin-deficient muscle is not well known. In this study, we aimed to verify the role of MMP-2 in dystrophin-deficient muscle by using *mdx* mice with genetic ablation of MMP-2 (*mdx*/MMP-$2^{-/-}$). We found impairment of regenerated muscle fiber growth with reduction of angiogenesis in *mdx*/MMP-$2^{-/-}$ mice at 3 months of age. Expression of vascular endothelial growth factor-A (VEGF-A), an important angiogenesis-related factor, decreased in *mdx*/MMP-$2^{-/-}$ mice at 3 months of age. MMP-2 had not a critical role in the degradation of dystrophin-glycoprotein complex (DGC) components such as β-dystroglycan and β-sarcoglycan in the regeneration process of the dystrophic muscle. Accordingly, MMP-2 may be essential for growth of regenerated muscle fibers through VEGF-associated angiogenesis in dystrophin-deficient skeletal muscle.

INTRODUCTION

Duchenne muscular dystrophy (DMD) is the most common severe X-linked muscular disorder, characterized by progressive muscle wasting and weakness (1). DMD is caused by a mutation in the *DMD* gene encoding the large cytoskeletal protein dystrophin (2). Dystrophin localizes to the sarcolemma of muscle fibers and forms a dystrophin-glycoprotein complex (DGC) with dystroglycans, sarcoglycans, and syntrophin-dystrobrevin complexes, and DGC links the cytoskeletal protein actin to the basal lamina of muscle fibers (3). DGC may play a role in membrane stabilization during muscle contraction or act as a transducer of signals from the extracellular matrix (ECM) to the muscle cytoplasm via its interactions with intracellular signaling molecules (4). The loss of dystrophin leads to a condition in which the membrane is leaky under mechanical stress, and the subsequent increase in Ca^{2+} permeability results in activation of various proteases and alteration of the expression or function of dystrophin-associated plasma membrane proteins, such as neuronal nitric oxide synthase (nNOS), aquaporin-4, and ion channels (5). The pathology of dystrophic muscle includes degeneration, necrosis with inflammatory cell invasion, regeneration, and fibrous and fatty changes. However, the underlying mechanisms of ECM degradation, inflammation, and fibrosis remain poorly understood.

ECM components have important roles in homeostasis and maintenance of muscle fiber functional integrity. Matrix metalloproteases (MMPs), a family of zinc-dependent endopeptidases, are key regulatory molecules in the formation, remodeling, and degradation of ECM components in both physiological and pathological processes (6,7),

such as tumor progression and metastasis, cerebrovascular and cardiovascular diseases, and rheumatoid arthritis (8). Among the MMPs, MMP-2 (also called gelatinase A) and MMP-9 (also called gelatinase B) are involved in ECM remodeling of skeletal muscle and in the dystrophic pathology of *mdx*, a mouse model for DMD (9). MMP-9 is produced by neutrophils and macrophages and is able to process β-dystroglycan, resulting in disruption of the link between the ECM and cell membrane in dystrophin-deficient skeletal muscle from DMD patients (10–12). We previously reported that MMP-9 over-expresses in *mdx* skeletal muscle after physical exercise (13) and may primarily be involved in the inflammatory process during muscle degeneration (14). Recently, it was reported that deletion of the *MMP9* gene in *mdx* mice reduces muscle inflammation and fibronecrosis, resulting in an improvement in muscle function (15). Based on these reports, MMP-9 may play an important role in ECM degradation in dystrophin-deficient muscle.

MMP-2 is derived from vascular endothelial cells as well as smooth muscle cells and has a role in angiogenesis, based on observation of impaired angiogenesis in an ischemic model in MMP-2 knockout mice (16). We and other researchers have also demonstrated that MMP-2 may be associated with ECM remodeling during muscle regeneration and fiber growth (9,14). Moreover, MMP-2 may be involved in myogenesis (17) and muscle regeneration (18). However, the precise role of MMP-2 has not been fully elucidated in dystrophic muscle. To better understand the role of MMP-2 in dystrophic pathology, we generated *mdx*/MMP-$2^{-/-}$ mice by crossing *mdx* with MMP-2 knockout (MMP-$2^{-/-}$) mice and examined the muscle pathology. Here, we demonstrate that MMP-2 ablation in *mdx* mice results in impairment of muscle fiber growth related to

down-regulation of vascular endothelial growth factor-A (VEGF-A) compared to *mdx*/MMP-$2^{+/+}$ mice. Moreover, expression of nNOS in 3-month-old *mdx*/MMP-$2^{-/-}$ mice was significantly lower than in *mdx* mice. These results imply that MMP-2 may be required for growth of regenerated muscle fibers through angiogenesis by VEGF-A (hereafter, VEGF) in dystrophin-deficient muscle.

RESULTS

MMP-2 ablation in *mdx* mice impairs growth of regenerated muscle fibers

To elucidate the role of MMP-2 in dystrophin-deficient muscle, we crossed MMP-2 knockout (MMP-$2^{-/-}$) mice (19) with *mdx* mice with the genetic background of C57 BL/6J to generate *mdx*/MMP-$2^{-/-}$ mice. MMP-2 mRNA and its protein activity were absent in the skeletal muscle of both MMP-$2^{-/-}$ and *mdx*/MMP-$2^{-/-}$ mice, but not in wild-type and *mdx* mice (Suppl. Fig.1A, C). There was no statistically significant difference in the MMP-9 mRNA level in the skeletal muscle between the groups at 1 and 3 months of age (Suppl. Fig.1B). Although we could not detected MMP-9 protein activity on gelatin zymography in mice aged 3 months (Suppl. Fig.1C), the levels of both the pro- and active-forms of MMP-9 protein levels were found to be significantly increased in *mdx* and *mdx*/MMP-$2^{-/-}$ mice as compared to the wild-type and MMP-$2^{-/-}$ mice at both 1 and 3 months of age (Suppl. Fig.1D-F). The discrepancy between the mRNA and protein levels of MMP-9 in dystrophic skeletal muscle is speculated to be due to post-transcriptional regulation (20). MMP-3 mRNA levels were significantly elevated in the skeletal muscle of *mdx* and *mdx*/MMP-$2^{-/-}$ mice at 1 and 3 months of age compared to that of the wild-type mice; the level was greatly

increased in *mdx*/MMP-2$^{-/-}$ mice at 3 months of age (Suppl. Fig.1G). The mRNA levels of tissue inhibitor of metalloproteinase (TIMP) -1, an intrinsic inhibitor of MMP-9 and -3, were significantly up-regulated in the skeletal muscle of *mdx* and *mdx*/MMP-2$^{-/-}$ mice compared to that of the wild-type mice at 1 and 3 months of age (Suppl. Fig.1H). There was no difference in the mRNA levels of TIMP-2, an intrinsic inhibitor of MMP-2, among the mouse groups at 1 or 3 months of age (Suppl. Fig.1I). In both MMP-2$^{-/-}$ mice (19) and *mdx*/MMP-2$^{-/-}$ mice, fertility and development were glossy normal. There were no differences in body weight at 1 or 3 months of age between *mdx* and *mdx*/MMP-2$^{-/-}$ or between wild-type and MMP-2$^{-/-}$ mice (Supp. Fig. 2A). Muscle power, evaluated using the hanging wire test and serum creatine kinase (CPK) levels, in *mdx*/MMP-2$^{-/-}$ at 3 months of age was not statistically different from that of *mdx* at the same age (Supp. Fig. 2B, C).

We then examined the histopathology of skeletal muscle from *mdx*/MMP-2$^{-/-}$ mice. A previous study of *mdx* mice reported muscle necrosis with infiltration of neutrophils or macrophages at around 2 weeks of age, massive muscle degeneration/necrosis at around 1 month of age, and completion of muscle necrosis with substitution of many regenerated fibers at 3 months of age (21). Histopathological findings for tibialis anterior (TA) muscle from *mdx*/MMP-2$^{-/-}$ mice at 1, 2, and 3 months of age were roughly comparable to those of *mdx* mice at each age (Fig. 1A). However, we found that the muscle fibers, especially the centronuclear regenerated fibers, in *mdx*/MMP-2$^{-/-}$ mice at 3 months of age were significantly smaller than in *mdx* mice at the same age (Fig. 1B–E). Almost all of the small regenerated fibers in *mdx*/MMP-2$^{-/-}$ mice at 3 months of age were type II fibers, and a similar tendency was observed in *mdx* mice at the same age (Supp. Fig. 2D). We also

analyzed diaphragm, quadriceps and gastrocnemius muscle in *mdx* and *mdx*/MMP-2$^{-/-}$ mice at 1 and 3 months of age. Like the TA muscle, these skeletal muscles in *mdx*/MMP-2$^{-/-}$ mice at 3 months of age exhibited impaired growth of regenerated fibers (Supp. Fig. 3). Furthermore, we monitored the muscle regeneration process as a result of cardiotoxin injury in skeletal muscle of MMP-2$^{-/-}$ mice at 6 weeks of age. The result clearly indicated that the centronuclear regenerating fibers 7 days after cardiotoxin injection in the skeletal muscle of MMP-2$^{-/-}$ mice were smaller than those of the wild-type (Supp. Fig. 4). These results suggest that ablation of MMP-2 may impair the growth of regenerated muscle fibers after the damage.

MMP-2 deficiency impairs angiogenesis in regenerated skeletal muscles of *mdx*

It has been reported that MMP-2 may be associated with angiogenesis, based on inhibition studies of MMP-2 (22,23). MMP-2 knockout mice have shown impairment of angiogenesis in an ischemia-induced model (16) and in a tumor model (24). To determine whether angiogenesis was impaired in the skeletal muscle of *mdx*/MMP-2$^{-/-}$ mice, we examined vessels in the TA muscle, through immunohistochemistry using an antibody to PECAM-1: an epithelial cell marker (Fig. 2A). We found that the mean size of vessels was significantly smaller in the skeletal muscle of *mdx*/MMP-2$^{-/-}$ mice at 3 months of age than that of age-matched *mdx* mice (Fig. 2B). Although the number of vessels per square millimeter was not different, the vessel counts per myofiber were significantly higher in *mdx* mice at 3 month of age, but decreased in age-matched *mdx*/MMP-2$^{-/-}$ mice (Fig. 2C, D). We also determined the endothelial area, which is equivalent to vascular bed, by multiplying the

size of vessels by their number in TA muscle. The endothelial area in *mdx*/MMP-2$^{-/-}$ mice at 3 months of age was significantly lower than that of the *mdx* mice at the same age (Fig. 2E). These results clearly indicate that MMP-2 ablation impairs angiogenesis in *mdx* skeletal muscle.

MMP-2 ablation in *mdx* mice down-regulates vascular endothelial growth factor

We found that ablation of MMP-2 caused growth impairment of regenerated fibers and of angiogenesis in *mdx* skeletal muscle at 3 months of age. We hypothesized that the growth impairment might be associated with the abnormality in angiogenesis; therefore, we examined the mRNA levels of various angiogenesis-related factors such as angiopoietin-1 and -2, platelet-derived growth factor (PDGF), fibroblast growth factor (FGF), transforming growth factor-β (TGF-β), and VEGF. No statistical differences in the levels of angiopoietin-1 or -2, PDGF, or FGF were detected between *mdx* and *mdx*/MMP-2$^{-/-}$ mice or between wild type and MMP-2$^{-/-}$ mice at 1 or 3 months of age (Fig. 3A–C, E). TGF-β mRNA levels were increased in *mdx* and *mdx*/MMP-2$^{-/-}$ mice compared with wild-type, but did not significantly change with or without MMP-2 (Fig. 3D). However, we found a significant decrease in the VEGF mRNA level in *mdx*/MMP-2$^{-/-}$ mice compared to *mdx* mice at 3 months of age (Fig. 3F). We also found a significant decrease in the mRNA level of Flt-1 (VEGF receptor 1), but not Flk-1 (VEGF receptor 2), in *mdx*/MMP-2$^{-/-}$ mice at 3 months of age (Fig. 3G, H). The VEGF protein level was significantly lower in skeletal muscle of *mdx*/MMP-2$^{-/-}$ mice compared to *mdx* mice at 3 months of age (Fig. 4A, B). VEGF was localized at neural cell adhesion molecule (NCAM)-positive muscle satellite

cells and at the sarcolemma in the same muscle fibers (Fig. 4C), but not at Mac-3 positive macrophages (Supp. Fig. 5). Flt-1 was also localized at most of the NCAM-positive muscle satellite cells. Flk-1 positive cells were identified as vascular endothelial cells by immunoreactivity of PECAM-1 (Fig. 4C). There were no differences in the localizations of VEGF, Flt-1, or Flk-1 between *mdx*/MMP-2$^{-/-}$ and *mdx* mice (Fig. 4C).

It has also been reported that MMP-2 is up-regulated in muscle regeneration in an experimentally injured model (9) and plays a role in myogenesis (17). To determine whether myogenic or growth factors are involved in pathogenesis in *mdx*/MMP-2$^{-/-}$ mice, we investigated the mRNA levels of the myogenic transcription factors Pax-3 and -7, MyoD, Myf5, myogenin, and MEF2 in the skeletal muscle. However, there were no statistical differences in the levels of these factors between *mdx* and *mdx*/MMP-2$^{-/-}$ mice or between wild type and MMP-2$^{-/-}$ mice at 1 or 3 months of age (Supp. Fig. 6A–F). There were also no differences in the mRNA levels of the growth factors insulin-like growth factor (IGF), myostatin, or follistatin in TA muscles between the two groups (Supp. Fig. 6G–I).

Overexpression of S100 proteins and cytokines in the skeletal muscle of *mdx*/MMP-2$^{-/-}$ mice at 3 months of age

As reported above, we examined the expression levels of various factors related to angiogenesis, myogenesis, and growth in the skeletal muscle of *mdx*/MMP-2$^{-/-}$ mice. To determine whether other genes affect pathology in *mdx*/MMP-2$^{-/-}$ mice, we conducted microarrays to comprehensively identify differentially expressed genes in the skeletal

muscle of *mdx* and *mdx*/MMP-2$^{-/-}$ mice at 1 and 3 months of age. Based on the profiles of all the genes, we found 113 genes that were differentially (> 2- or < 0.5-fold) affected by MMP-2 ablation (Supp. Table 1). Thirteen genes were up-regulated (Supp. Table 2) and 18 genes were down-regulated (Supp. Table 3) at 1 month of age, and 69 genes were up-regulated (Supp. Table 4) and 13 genes were down-regulated (Supp. Table 5) at 3 months of age in *mdx*/MMP-2$^{-/-}$ mice compared with *mdx* mice (Supp. Fig. 7A, B). The genes that were up-regulated at 3 months of age in *mdx*/MMP-2$^{-/-}$ mice were mainly involved with protein binding, cytokine and its receptor, or cell growth. Among the genes up-regulated at 3 months of age, S100 calcium-binding protein A8 (S100A8) and A9 (S100A9); cytokines such as chemokine C-C motif ligand (CCL)-2 and-7, chemokine C-C motif receptor (CCR)-1 and -2, and chitinase 3-like 3 were highly up-regulated in *mdx*/MMP-2$^{-/-}$ mice (Supp. Table 4). We confirmed these results by using quantitative real-time PCR (Supp. Fig. 7C–G).

MMP-2 ablation further decreases nNOS expression in the skeletal muscle of *mdx* mice

Nitric oxide (NO) is a vasodilator produced by nitric oxide synthase (NOS), and inhibition of NOS activity abolishes capillary proliferation in electrically stimulated skeletal muscle (25). In electrical stimulated skeletal muscle, expression of endothelial NOS (eNOS) and neuronal NOS (nNOS) increase in the early and late stages of angiogenesis, respectively (25–27). nNOS is linked to DGC, and dystrophin deficiency causes a reduction in nNOS expression at the sarcolemma, resulting in modification of dystrophic pathology (28,29).

Thus, we examined the mRNA levels of nNOS, eNOS, and inducible NOS (iNOS) produced by invaded inflammatory cells in the skeletal muscle of *mdx*/MMP-2$^{-/-}$ mice. mRNA expression of nNOS, but not of eNOS and iNOS, was significantly lower in *mdx*/MMP-2$^{-/-}$ than in *mdx* mice at 3 months of age (Fig. 5A–C). Western blotting also revealed that the nNOS protein level was significantly lower in *mdx*/MMP-2$^{-/-}$ than in *mdx* mice at 3 months of age (Fig. 5D, E), although there were no apparent differences in nNOS immunoreactivity between the *mdx*/MMP-2$^{-/-}$ and *mdx* mice (Fig. 5F). These results suggest that down-regulation of nNOS in the regenerated skeletal muscle of *mdx*/MMP-2$^{-/-}$ mice may influence impairment of angiogenesis.

MMP-2 does not affect the degradation of DGC components in the process of dystrophic muscle regeneration

Dystroglycans (DGs) comprise two subunits, a highly glycosylated extracellular matrix protein, α-dystroglycan (α-DG), and a transmembrane protein, β-dystroglycan (β-DG). DGs are membrane receptors involved with the complex of glycoproteins associated with dystrophin (30), and their interaction is crucial in maintaining the integrity of the plasma membrane. In dystrophin-deficient muscle, the interaction between the two DG subunits may be disrupted by the proteolytic activity of MMPs (12). Previous research has examined the proteolytic activities of human MMP-9 and MMP-2 on the recombinant extracellular domain of β-DG and characterized a cleavage site by MMP-9 on β-DG (31). However, the molecular mechanism underlying the effect of MMP-2 is still unknown. We examined whether MMP-2 ablation in *mdx* mice affects processing of DGC in the skeletal muscle. In

the skeletal muscle of both *mdx* and *mdx*/MMP-2$^{-/-}$ mice at 1 and 3 months of age, full-length 43-kDa β-DG (βDG_{43}) was cleaved to a 30-kDa form of β-DG (βDG_{30}) (Fig. 6A); however, although the degree of degradation in *mdx*/MMP-2$^{-/-}$ mice was less than that in *mdx* mice at 1 month of age, it was not different at 3 months of age (Fig. 6B, C). Similary, the expression of β-sarcoglycan did not change in the skeletal muscle of *mdx*/MMP-2$^{-/-}$ mice at 1 or 3 months of age compare to *mdx* of the same age (Supp. Fig. 8). In the process of regeneration of dystrophic muscle, MMP-2 may not have a critical role in the degradation of DGC components.

DISCUSSION

In this study, we investigated the role of MMP-2 in dystrophic skeletal muscle using *mdx* mice with MMP-2 ablation (*mdx*/MMP-2$^{-/-}$). The histopathology of skeletal muscle in *mdx*/MMP-2$^{-/-}$ mice at 3 months of age showed small regenerated muscle fibers and an impairment of angiogenesis compared to *mdx* mice at the same age. The impaired growth of regenerating muscle fibers was also observed in the cardiotoxin injury model of MMP-2$^{-/-}$ mice; suggesting that MMP-2 may play an important role in the muscle regeneration under certain disease conditions. MMP-2, a primary MMP derived from vascular endothelial cells and smooth muscle cells, degrades various ECM proteins (32,33), and is implicated as a key player in vascular development and angiogenesis (34). MMP-2 knockout mice have demonstrated a reduction in angiogenesis and corresponding tumor growth (24), and impairment of ischemia-induced neovascularization through a decreased number of endothelial cells and endothelial progenitor cells (16). Therefore, we

hypothesized that the close relationship between impairment of regenerated myofiber growth and reduction in angiogenesis in the *mdx*/MMP-2$^{-/-}$ mice might allow us to identify factors related to angiogenesis or growth in these mice. We subsequently found a reduction of VEGF expression in the regenerated skeletal muscle of the mice at 3 months of age.

VEGF plays an important role in mediating both physiological and pathological angiogenesis via inducing vasodilation or vascular permeability, and by stimulating the proliferation, migration, and survival of endothelial cells (35). In a previous study, both cultured satellite cells and myoblasts expressed VEGF, and VEGFR-1 and -2; furthermore, administration *in vitro* stimulates myoblast migration and survival, protects myogenic cells from apoptosis, and promotes myogenic cell growth (36). In normal muscles, VEGF and its receptors are expressed in vascular structures and not in muscle fibers; however, they are expressed in satellite cells and regenerating muscle fibers after experimental muscle damage, suggesting the operation of an autocrine pathway that may promote the survival and regeneration of myocytes (37). This study also demonstrates that the introduction of VEGF by using a virus vector promotes regeneration via angiogenesis, resulting in the decrease in muscle damage as well as the promotion of muscle regeneration and function in *mdx* mice (37). Meanwhile, another study shows that VEGF administration by using viral vectors injected in normal mouse skeletal muscle results in the appearance of a notable subset of muscle fibers exhibiting muscle regeneration. Moreover, the delivery of VEGF markedly promotes muscle fiber regeneration with a dose-dependent effect after experimental muscle damage with ischemia, glycerol, or cardiotoxin (38). Furthermore, the increased density of satellite cells has been observed adjacent to capillaries, suggesting a

possible role of VEGF in homing circulating progenitor germ cells to specific muscle location and/or in regulating the satellite cells pool (39). Taken together, VEGF might function during regeneration not only through neovascolarization but also by directly acting on muscle cells and on the recruitment of progenitor cells from bone marrow during dystrophic pathology. VEGF was down-regulated in an ischemic-induced model using MMP-2 knockout mice due to a reduction in the number of invasive macrophages producing VEGF (16). However, our data indicate that VEGF is localized in NCAM-positive satellite cells and the sarcolemma in certain muscle fibers (Fig. 4C), but not in Mac-3-positive macrophages (Supp. Fig. 5). In a recent report, MMP-2 transcriptional inactivation by using a siRNA-based approach both in *in vitro* and *in vivo* significantly reduced integrin-αVβ3-medaited phosphoinositied 3-kinase/AKT-induced VEGF expression, which ultimately decreased tumor cell-induced angiogenesis (40). Similar mechanism might also underlie the relationship between MMP-2 and VEGF in dystrophic muscle. Although VEGF is known to be located upstream of MMP-2, we suggest that MMP-2 and VEGF may regulate each other in the skeletal muscle.

We conducted microarrays to comprehensively identify differentially expressed genes in *mdx*/MMP-2$^{-/-}$ mice, because other genes could affect the phenotype. Among the genes up-regulated at 3 months of age in *mdx*/MMP-2$^{-/-}$ mice, S100A8 and A9 mRNA levels were significantly increased. S100 proteins are involved in the pathogenesis of cellular stress condition such as wound healing or inflammatory disorders (41). In particular, S100A8 and A9 are required for transcriptional activation of the *MMP-2* gene (42). We suggest, therefore, that over-expression of S100A8 and A9 in *mdx*/MMP-2$^{-/-}$ mice

may compensate for MMP-2 ablation. In addition, microarray analysis (Supp. Table 4) and real-time PCR revealed that MMP-3 was significantly increased in the skeletal muscle of *mdx*/MMP-2$^{-/-}$ mice at 3 months of age compared to that of the age-matched *mdx* mice. It has been reported that MMP-3 is significantly elevated in the synovium by intra-articular injection of recombinant S100A8 in knee joints of normal mice, and was increased in macrophages stimulated by recombinant S100A8 or S100A8/A9 heterodimer (43). The up-regulation of MMP-3 in skeletal muscle of *mdx*/MMP-2$^{-/-}$ mice at 3 months of age may be caused by overexpression of S100A8 and A9.

We also found that expression of nNOS in the *mdx*/MMP-2$^{-/-}$ mice was significantly lower than in *mdx* mice at 3 months of age. This further reduction in nNOS may have been caused by MMP-2 ablation in the *mdx* mice, or impairment of angiogenesis may secondarily induce a further decrease in nNOS. NO is increased in the ischemic hind limb and eliminating NO impairs the revascularization process (44). It has been reported that an nNOS transgene in *mdx* mice ameliorated muscular dystrophy (45) and that *mdx* mice expressed dystrophin only in smooth muscle cells, restoring vascular nNOS expression and NO-dependent vasoregulation and resulting in improvement in dystrophic pathology (46). Taken together, these studies show that MMP-2 ablation in *mdx* mice may result in further reduction of nNOS in dystrophic muscle, with a detrimental effect on the function and regeneration of dystrophic muscle. While it is reported that nNOS levels are reduced in inflammatory conditions (47). Actually, our data showed that the expression of some cytokines (e.g., CCL-2) was significantly increased in the skeletal muscle of *mdx*/MMP-2$^{-/-}$ at 3 months of age. Taken a report that S100A8/A9 enhances the gene

expression of pro-inflammatory proteins such as CCL-2 (48), S100A8/A9 up-regulation may enhance pro-inflammatory genes, resulting in the down-regulation of nNOS expression in *mdx*/MMP-2$^{-/-}$ mice at 3 months of age. Interestingly, nNOS$^{-/-}$ mice in an acute lung injury model show reduced expression of VEGF protein (49). The decrease in nNOS levels via increased cytokines may also reduce VEGF expression in the skeletal muscle of *mdx*/MMP-2$^{-/-}$ mice at 3 months of age.

We assessed differences in the degradation patterns of DGC in the skeletal muscles between *mdx* and *mdx*/MMP-2$^{-/-}$ mice. The β-DG degradation was reduced by MMP-2 ablation in *mdx* mice at 1 month of age. Nevertheless, at 3 months of age, β-DG degradation was unchanged in the presence of MMP-2. Previous reports documented that MMP-2 as well as MMP-9 were able to degrade β-DG (50), and that macrophage-derived MMP-2 in a mouse model of experimental autoimmune encephalomyelitis participated in tissue injury via β-DG degradation through proteolytic activity (10). However, our data indicated that β-DG degradation by MMP-2 was not apparent in the process of muscle regeneration. The expression of β-sarcoglycan remained unchanged in the skeletal muscle of *mdx*/MMP-2$^{-/-}$ mice at 1 and 3 months of age compared to *mdx* of the same age. These results suggest that the ablation of MMP-2 does not a significantly influence the degradation of β-dystroglycan and β-sarcoglycan in the regeneration process of the dystrophic muscle.

In this study, we found that reduction of angiogenesis via decreased VEGF and nNOS expression may impair regeneration in the skeletal muscle of *mdx* mice with MMP-2 ablation (Fig. 7). Corticosteroids are promising agents for the prevention of progression in

various diseases including DMD; however, they inhibit VEGF and MMP-2, resulting in a reduction of tissue angiogenesis (51,52). Normal rats treated with corticosteroids exhibit muscle atrophy and weakness with a concomitant reduction in VEGF expression (53,54); therefore, the decrease in MMP-2 and VEGF by corticosteroids might be associated with the pathogenesis in steroid myopathy.

MATERIALS AND METHODS

Mice

Control (strain: C57 BL/6J) and MMP-2-knockout (strain: C57BL/6J-Mmp2tm) mice were purchased from Jackson Laboratory (Bar Harbor, ME). Dystrophin-deficient (*mdx*) mice (strain: C57BL/6J-DMD*mdx*) were a gift from the Institute of Neuroscience, National Research Center of Neurology and Psychiatry (Tokyo, Japan). MMP-2-knockout (MMP-$2^{-/-}$) mice were crossed with *mdx* mice to generate littermate wild-type (WT), MMP-$2^{-/-}$, *mdx*/MMP-$2^{+/+}$, and *mdx*/MMP-$2^{-/-}$ mice. All genotypes were determined using PCR analysis of mice tail DNA. An amplification-resistant mutation system assay was used to identify control and *mdx* mice (55). MMP-2 knockout and control mice were identified using the primer sets suggested by the Jackson Laboratory. Mice were housed in a plastic cage in a temperature-controlled environment with a 12-hour light/dark cycle and free access to food and water. All experiments with animals were carried out in accordance with institutional guidelines, and approved by the institutional review board of Shinshu University, Japan.

Muscle tissue extraction and preparation

TA muscles were carefully dissected and frozen in isopentane cooled by liquid nitrogen for histological and immunohistochemical analyses and protein and RNA isolation, and were stored at -80 °C. Ten-micrometer transverse cryostat sections were cut in the center of the TA muscle belly to obtain the largest cross-sectional area (CSA), placed on slides, air dried, and stained with hematoxylin and eosin (H&E). Serial sections were stained to demonstrate

myofibrillar ATPase activity. Diaphragm, quadriceps, and gastrocnemius muscles were also dissected and frozen, and were stained with H&E as noted above. The sections were viewed and photographed using a digital camera system (Leica Microsystems, Wetzlar, Germany).

Cardiotoxin muscle injury and histochemistry

We injected 100 μL cardiotoxin (10 mM in 0.9% NaCl) (Sigma, St. Louis, MO, USA) into the TA muscle of wild-type and MMP-$2^{-/-}$ mice at 6 weeks of age using a 27-gauge needle and a 1-mL syringe. The needle was inserted deep into the TA muscle longitudinally toward the knee from the ankle. The needle was held in place for a few seconds and then slowly withdrawn along the long axis of the anterior tibial muscle with a little pressure to allow the cardiotoxin to permeate throughout the muscle. The TA muscles were isolated before the injection, and 3 and 7 days after; the muscles were then frozen in liquid nitrogen-cooled isopentane. Ten-micrometer transverse cryostat sections were stained with hematoxylin and eosin (H&E), and the diameters of 500 muscle fibers were measured.

Morphometric analysis

Morphometric analysis was performed to determine the CSA of each muscle fiber by using the H&E-stained TA, diaphragm, quadriceps, and gastrocnemius muscle sections, separately recording the CSAs for perinuclear fibers and centronuclear regenerated fibers. Necrotic fibers, when present, were discarded. The distribution of muscle fiber CSAs was examined using National Institutes of Health (Bethesda, MD) images. At least 1000 fibers were analyzed for each muscle, and muscle fiber boundaries were determined to count the

size and number of the fibers. All images were obtained under identical conditions and at the same magnification. For the CSA histogram, histological parameters were evaluated and treated as previously described (56). Variability in fiber size was determined by the mean ± S.E.M.

Study for vessels was performed on 6-μm-thick TA muscle sections stained with anti-PECAM-1 antibody. Serial H&E-stained sections were used to count the number of muscle fibers. The number and size of each vessel, and number of muscle fibers were counted under identical conditions and at same magnification. We determined the number of vessels per myofiber, and endothelial area of PECAM-1-positive vessels in total area.

Immunohistochemical analysis

For immunofluorescent staining, serial cross sections (6-μm thick) from frozen skeletal muscle tissues were mounted on glass slides. The sections were air dried and blocked in 10% goat serum in phosphate-buffered saline (PBS) for 30 min, and incubated with primary antibodies in blocking solution at 4 °C overnight. The sections were washed briefly with 1× PBS before incubation with secondary antibodies for 1 h at room temperature and then washed three times for 30 min with 1× PBS. The slides were mounted using a fluorescence medium with 4',6-diamidino-2-phenylindole (DAPI; Vector Laboratories, Burlingame, CA), visualized using a fluorescent microscope (Olympus, Tokyo, Japan), and images were captured using a VB-7010 camera (Keyence, Osaka, Japan). The primary antibody dilutions and sources were as follows: rat monoclonal anti-PECAM-1 (1:50; BD Transduction Laboratories, San Jose, CA), rabbit polyclonal anti-VEGF-A (1:50; Santa Cruz

Biotechnology, Santa Cruz, CA), rabbit polyclonal anti-Flt-1 (1:100; Santa Cruz Biotechnology), rabbit monoclonal anti-Flk-1 (1:100; Cell Signaling Technology, Danvers, MA), rat monoclonal anti-laminin α2-chain (1:100; Enzo Life Sciences, Plymouth Meeting, PA), rabbit polyclonal anti-nNOS (1:200; Invitrogen, Carlsbad, CA), rat monoclonal anti-NCAM (1:100; Millipore, Billerica, MA), rat monoclonal anti-Mac3 (1:50 BD; Transduction Laboratories), mouse anti-β-sarcoglycan (1:200; Leica Microsystems). Alexa Fluor® 488 or Alexa Fluor® 568-conjugated secondary antibodies were obtained from Invitrogen and used at 1:500 dilution.

Total protein extract and western blotting

Muscle tissues (20 mg) were homogenized in 150 μL of 5% sodium dodecyl sulfate (SDS) sample buffer (50 μmol/L Tris-HCl, pH 8.0, 10 μmol/L ethylenediaminetetraacetic acid, 5% SDS, and 5% β-mercaptoethanol). After centrifugation (10 min at 15,000 *g*), the protein concentration was estimated in the supernatant using the BCA protein assay kit (Bio-Rad, Hercules, CA). Protein homogenates recovered from the supernatant from each sample were denatured for 5 minutes at 95 ºC in reducing buffer (50 μL of SDS buffer containing 5% SDS, 0.01% bromophenol blue, 10% glycerol, and 5% β-mercaptoethanol). Protein extracts (10 μg/lane) were submitted to SDS-polyacrylamide gel electrophoresis (7.5% or 12.5%) with pre-stained standard proteins (Bio-Rad) to achieve more accurate molecular weight determination. The resulting gel was transferred onto a 0.2-μm nitrocellulose membrane (Millipore) using a transfer buffer (25 mmol/L Tris-HCl, pH 8.3, 192 mmol/L glycine, and 20% methanol). The membranes were blocked with Tris-buffer, 0.1% Tween

20 (TBST) containing 5% milk (w/v) for 1 h at room temperature. All membranes were incubated with primary antibodies at 4 °C overnight followed by several washes with TBST. The membranes were incubated with peroxidase-conjugated secondary antibodies (Bio-Rad) for 1 h, washed several times with the washing buffer described above, and visualized using an enhanced chemiluminescence system according to the manufacturer's protocol (Amersham, Little Chalfont, UK). Protein signals were quantified by scanning densitometry using the National Institutes of Health (Bethesda, MD) program package. The results from each experimental group were expressed as integrated intensities relative to the control samples. Equal loading of proteins was assessed on stripped blots by immunodetection using the anti-glyceraldehyde-3-phosphate dehydrogenase (GAPDH) antibody. The primary antibody dilutions and sources were as follows: goat anti-VEGF-A (1:200; Santa Cruz Biotechnology), mouse anti-nNOS (1:1,000; BD Transduction Laboratories), rabbit anti-MMP-9 (1:1,000; Millipore), mouse anti-β-dystroglycan (1:800; Leica Microsystems), mouse anti-β-sarcoglycan (1:400; Leica Microsystems), mouse anti-GAPDH (1:3,000; Millipore).

Gelatin zymography

Frozen skeletal muscles were homogenized in an extraction buffer (62.5 mM Tris-HCl [pH 6.8], 2% sodium dodecyl sulfate [SDS], and 10% glycerol), and total protein content was assessed using a BCA protein assay kit (Bio-Rad). Each extract (50 μg) was dissolved in a loading buffer provided by the manufacture and subsequently electrophoresed through a gelatin-containing SDS polyacrylamide gel provided as part of the gelatin zymography kit

(Invitrogen). The gel was washed with regenerating buffer and subsequently incubated for 24 hours at 37°C in developing buffer that was also provided by the manufacture. The gels were stained in Coomasie Brilliant Blue (CBB) and destained with a destaining solution (Bio-Rad). Gelatinolytic activity was identified as clear bands on a blue background. Gelatin zymography detects the activity of both active and pro-form gelatinolytic MMPs. This is because exposure to SDS during gel electrophoresis activates the pro-form MMPs without proteolytic cleavage of the prodomain. Equality of the protein concentration was confirmed by CBB staining. Myosin heavy chain (MHC) was used as a loading control.

RNA isolation and gene expression profiling

Frozen tissues (20 mg) for each muscle were homogenized and the total RNA isolated using an RNeasy Fibrous Tissue Kit (Qiagen, Hilden, Germany) according to the manufacturer's instructions. cDNA synthesis, biotin-labeled target synthesis, Mouse Genome 430 2.0 Array Gene Chip (Affymetrix, Santa Clara, CA) array hybridization, staining, and scanning were performed according to standard protocols supplied by Affymetrix. The quality of the data was controlled using Microarray Suite MAS 5.0 (Affymetrix). The MAS-generated raw data were uploaded to GeneSpring GX software version 10 (Silicon Genetics, Redwood City, CA). The software calculated signal intensities, and each signal was normalized to the median of its values in all samples or the 50th percentile of all signals for a specific hybridization experiment. Fold ratios were obtained by comparing normalized data for *mdx* and *mdx*/MMP-$2^{-/-}$ mice.

Analyses by real-time polymerase chain reaction

First-strand cDNA was synthesized using a QuantiTect reverse transcription kit (Qiagen). The levels of mRNA and 18S rRNA were quantified using fluorescent dye SYBR-green detection (Roche Diagnostics, Basel, Switzerland) with 10 nM of each primer at a final volume of 10 μL, and the reactions were carried out in duplicate using the StepOnePlus RT-PCR system (Applied Biosystems, Foster City, CA). Thermal cycling conditions for all primers were 10 min at 95 ºC, then 40 cycles each of 15 s at 94 ºC, 30 s at 48 ºC, 1 min at 72 ºC, and a final extension of 10 min at 72 ºC. For each gene, all samples were amplified simultaneously. Each RNA quantity was normalized to its respective 18S rRNA mRNA quantity. Primer sequences for RT-PCR are shown in Supp. Table 1.

Statistical analysis

Results are expressed as means ± S.E.M. Statistical analysis was performed using an unpaired *t*-test for two-group comparisons, and multiple comparisons were performed using a one-way ANOVA. Intergroup comparison was carried out using the Bonferroni correction. Statistical significance was set at $p < 0.05$. Statistical analyses were carried out using the software SigmaStat, version 2.0 (Aspire Software, Ashburn, VA).

SUPPLEMENTARY MATERIAL

Supplementary material is available at *HMG* online.

FUNDING

This work was supported by Grants-in-Aid for Scientific Research (B) from The Ministry of Education, Culture, Sports, Science and Technology of Japan [21300157 to A.N.].

ACKNOWLEDGMENTS

Conflict of Interest Statement: None declared.

REFERENCES

1. Emery, A.E. and Gosden, C. (1974) A neurogenic component in muscular dystrophy. *J. Med. Genet.*, **11**, 76–79.
2. Hoffmann, E.P., Monaco, A.P., Feener, C.C. and Kunkel, L.M. (1987) Conservation of the Duchenne muscular dystrophy gene in mice and humans. *Science*, **238**, 347–350.
3. Ervasti, J.M. and Campbell, K.P. (1991) Membrane organization of the dystrophin-glycoprotein complex. *Cell*, **66**, 1121–1131.
4. Ibraghimov-Beskrovnaya, O., Ervasti, M.J., Leveille, J.C., Slaughter, A.C., Sernett, W.S. and Campbell, P.K. (1992) Primary structure of dystrophin-associated glycoproteins linking dystrophin to the extracellular matrix. *Nature*, **355**, 696–702.
5. Allen, D.G., Whitehead, N.P. and Yeung, E.W. (2005) Mechanisms of stretch-induced muscle damage in normal and dystrophic muscle: role of ionic changes. *J. Physiol.*, **567**, 723–735.
6. Mott, J.D. and Werb, Z. (2004) Regulation of matrix biology by matrix metalloproteinases. *Curr. Opin. Cell Biol.*, **16**, 558–564.
7. Vu, T.H. and Werb, Z. (2000) Matrix metalloproteinases: effectors of development and normal physiology. *Genes Dev.*, **14**, 2123–2133.
8. Nagase, H. and Woessner, J.F. Jr. (1999) Matrix metalloproteinases. *J. Biol. Chem.*, **274**, 21491–21494.
9. Kherif, S., Lafuma, C., Dehaupas, M., Lachkar, S., Fournier, J.G., Verdiere-Sahuque, M., Fardeau, M. and Alameddine, H.S. (1999) Expression of matrix metalloproteinase 2 and 9 in regenerating skeletal muscle: a study in experimentally injured and *mdx*

muscles. *Dev. Biol.*, **205**, 158–170.

10. Agrawal, S., Anderson, P., Durbeej, M., Rooijen, N., Ivars, F., Opdenakker, G. and Sorokin, L.M. (2006) Dystroglycan is selectively cleaved at the parenchymal basement membrane at sites of leukocyte extravasation in experimental autoimmune encephalomyelitis. *J. Exp. Med.*, **203**, 1007–1019.
11. Zhong, D., Saito, F., Saito, Y., Nakamura, A., Shimizu, T. and Matsumura, K. (2006) Characterization of the protease activity that cleaves the extracellular domain of β-dystroglycan. *Biochem. Biophys. Res. Commun.*, **345**, 867–871.
12. Matsumura, K., Zhong, D., Saito, F., Arai, K., Adachi, K., Kawai, H., Higuchi, I., Nishino, I. and Shimizu, T. (2005) Proteolysis of β-dystroglycan in muscular disease. *Neuromuscul. Disord.*, **15**, 336–341.
13. Nakamura, A., Yoshida, K., Ueda, H., Takeda, S. and Ikeda, S. (2005) Up-regulation of mitogen activated protein kinases in *mdx* skeletal muscle following chronic treadmill exercise. *Biochim. Biophys. Acta*, **1740**, 326–331.
14. Fukushima, K., Nakamura, A., Ueda, H., Yuasa, K., Yoshida, K., Takeda, S. and Ikeda, S. (2007) Activation and localization of matrix metalloproteinase-2 and -9 in the skeletal muscle of the muscular dystrophy dog ($CXMD_J$). *BMC Musculoskelet. Disord.*, **8**, 1–11.
15. Li, H., Mittal, A., Makonchuk, D.Y., Bhatnagar, S. and Kumar, A. (2009) Matrix metalloproteinase-9 inhibition ameliorates pathogenesis and improves skeletal muscle regeneration in muscular dystrophy. *Hum. Mol. Genet.*, **18**, 2584–2598.
16. Chen, X.W., Kuzuya, M., Nakamura, K., Maeda, K., Tsuzuki, M., Kim, W., Sasaki, T.,

Liu, Z., Inoue, N., Kondo, T., Jin, H., Numaguchi, Y., Okumura, K., Yokota, M., Iguchi, A. and Murahara, T. (2007) Mechanisms underlying the impairment of ischemia-induced neovascularization in matrix metalloproteinase 2-deficient mice. *Circ. Res.*, **100**, 904–913.

17. Lluri, G. and Jaworski, E.M. (2005) Regulation of TIMP-2, MT1-MMP, and MMP-2 expression during C2C12 differentiation. *Muscle Nerve*, **32**, 492–499.
18. Zimowska, M., Brzoska, E., Swierczynska, M., Streminska, W. and Moraczewski, J. (2008) Distinct patterns of MMP-9 and MMP-2 activity in slow and fast twitch skeletal muscle regeneration *in vivo*. *Int. J. Dev. Biol*., **52**, 307–314.
19. Itoh, T., Ikeda, T., Gomi, H., Nakao, S., Suzuki, T. and Itohara, S. (1997) Unaltered secretion of β-amyloid precursor protein in gelatinase A (matrix metalloproteinase 2)-deficient mice. *J. Biol. Chem.*, **272**, 22389–22392.
20. Fähling, M., Steege, A., Perlewitz A., Nafz, B., Mrowka, R., Persson, P.B. and Thiele B.J. (2005) Role of nucleolin in posttranscriptional control of MMP-9 expression. *Biochim. Biophys. Acta*, **1731**, 32–40.
21. Gillis, J.M. (1999) Understanding dystrophinopathies: an inventory of the structural and functional consequence of the absence of dystrophin in muscles of the *mdx* mouse. *J. Muscle. Res. Cell. Motil.*, **20**, 605–625.
22. Collen, A., Hanemaaijer, R., Lupu, F., Quax, PH., van Lent, N., Grimbergen, J., Peters, E., Koolwijk, P. and Hinsbergh, V.W. (2003) Membrane-type matrix metalloproteinase-mediated angiogenesis in a fibrin-collagen matrix. *Blood*, **101**, 1810–1817.

23. Silletti, S., Kessler, T., Goldberg, J., Boger, D.L. and Cheresh, D.A. (2001) Disruption of matrix metalloproteinase 2 binding to integrin alpha v beta 3 by an organic molecule inhibits angiogenesis and tumor growth in vivo. *Proc. Natl. Acad. Sci. U.S.A.*, **98**, 119–124.
24. Itoh, T., Tanioka, M., Yoshida, H., Yoshioka, T., Nishimoto, H. and Itohara, S. (1998) Reduced angiogenesis and tumor progression in gelatinase A-deficient mice. *Cancer Res.*, **58**, 1048–1051.
25. Milkiewicz, M., Hudlicka, O., Brown, M.D. and Silgram, H. (2005) Nitric oxide, VEGF and VEGFR-2: interactions in activity-induced angiogenesis in rat skeletal muscle. *Am. J. Physiol.*, **289**, H336–H343.
26. Reiser, P.J., Kline, W. and Vaghy, P.L. (1997) Induction of neuronal type nitric oxide synthase in skeletal muscle by chronic electrical stimulation in vivo. *J. Appl. Physiol.*, **83**, 1250–1255.
27. Hudlicka, O. and Brown, M.D. (2009) Adaptation of skeletal muscle microvasculature to increased or decreased blood flow: role of shear stress, nitric oxide and vascular endothelial growth factor. *J. Vasc. Res.*, **46**, 504–512.
28. Brenman, J.E., Chao, D.S., Xia, H., Aldape, K. and Bredt, D.S. (1995) Nitric oxide synthase complexed with dystrophin and absent from skeletal muscle sarcolemma in Duchenne muscular dystrophy. *Cell*, **82**, 743–752.
29. Chang, W.J., Iannaccone, S.T., Lau, K.S., Masters, B.S.S., McCabe, T.J., McMillan, K., Padre, R.C., Spencer, M.J., Tidball, J.G. and Stull, J.T. (1996) Neuronal nitric oxide synthase and dystrophin-deficient muscular dystrophy. *Proc. Natl. Acad. Sci. U.S.A.*, **93**,

9142–9147.

30. Yamada, H., Saito, F., Fukuta-Ohi, H., Zhong, D., Hase, A., Arai, K., Okuyama, A., Maekawa, R., Shimizu, T. and Matsumura, K. (2001) Processing of β-dystroglycan by matrix metalloproteinase disrupts the link between the extracellular matrix and cell membrane via the dystroglycan complex. *Hum. Mol. Genet.*, **10**, 1563–1569.
31. Bozzi, M., Inzitari, R., Sbardell, D., Monaco, S., Pavoni, E., Gioia, M., Marini, S., Morlacchi, S., Sciandra, F., Castagnola, M., Giardina, B., Brancaccio, A. and Coletta, M. (2009) Enzymatic processing of b-dystroglycan recombinant ectodomain by MMP-9: identification of the main cleavage site. *IUBMB Life*, **61**, 1143–1152.
32. Haas, T.L., Davis, J. and Madri, J.A. (1998) Three-dimensional type I collagen lattices induce coordinate expression of matrix metalloproteinases MT1-MMP and MMP-2 in microvascular endothelial cells. *J. Biol. Chem.*, **273**, 3604–3610.
33. Kuzuya, M., Kanda, S., Sasaki, T., Mori, N., Chen, X.W., Itoh, T., Itohara, S. and Iguchi, A. (2003) Deficiency of gelatinase A suppression smooth muscle cell invasion and development of experimental intimal hyperplasia. *Circulation*, **108**, 1375–1381.
34. Kinoh, H., Sato, H., Tsunezuka, Y., Takino, T., Kawashima, A., Okada, Y. and Seiki, M. (1996) MT-MMP, the cell surface activator of proMMP-2 (pro-gelatinase A), is expressed with its substrate in mouse tissue during embryogenesis. *J. Cell. Sci.*, **109**, 953–959.
35. Matsumoto, T. and Claesson-Welsh, L. (2001) VEGF receptor signal transduction. *Sci. STKE*, **112**, 1–17.
36. Germani, A., Carlo, A.D., Mangori, A., Straino, S., Giacinti, C., Turrini, P., Biglioli, P.

and Capogrossi, C. (2003) Vascular endothelial growth factor modulates skeletal myoblast function. *Am. J. Pathol.*, **163**, 1417–1428.

37. Messina, S., Mazzeo, A., Bitto, A., Aguennouz, M., Migliorato, A., Pasquale, M.G., Minutoli, L., Altavilla, D., Zentilin, L., Giacca, M., Squandrito, F. and Vita, G. (2007) VEGF overexpression *via* adeno-associated virus gene transfer promotes skeletal muscle regeneration and enhances muscle function in *mdx* mice. *FASEB J.*, **21**, 3737–3746.
38. Arsic, N., Zacchigna, S., Zentilin, L., Ramirez-Correa, G., Pattarini, L., Salvi, A., Sinagra, G. and Giacca, M. (2004) Vascular endothelial growth factor stimulates skeletal muscle regeneration *in vivo*. *Mol. Ther.*, **10**, 844–854.
39. De Angelis, L., Berghella, L., Coletta, M., Lattanzi, L., Zanchi, M., Cusela-De Angelis, M.G., Ponzetto, C. and Cossu, G. (1999) Skeletal myogenic progenitors originating from embryonic dorsal aorta coexpress endothelial and myogenic markers and contribute to postnatal muscle growth and regeneration. *J. Cell Biol.*, **147**, 869–877.
40. Chetty, C., Lakka, S.S., Bhoopathi, P. and Rao, J. (2009) MMP-2 alters VEGF expression *via* αVβ3 integrin-mediated PI3K/AKT signaling in A549 lung cancer cells. *Int. J. Cancer*, **127**, 1081–1095.
41. Heizmann, C.W., Fritz, G. and Schafer, B.W. (2002) S100 proteins: structure, functions and pathology. *Front. Biosci.*, **7**, d1356–1368.
42. Yong, H.Y. and Moon, A. (2007) Role of calcium-binding proteins, S100A8 and S100A9, in invasive phenotype of human gastric cancer cells. *Arch. Pharm. Res.*, **30**, 75–81.

43. van Lent, P.L., Grevers, L.C., Blom, A.B., Arntz, O.J., Loo, van de F.A., Kraan, van der P., Abdollahi-Roodsaz, S., Srikrishna, G., Freeze, H., Sloetjes, A., Nacken, W., Vogl, T., Roth, J. and Berg, van den W.B. (2008) Stimulation of chondrocyte-mediated cartilage destruction by S100A8 in experimental murine arthritis. *Arthritis. Rheum.*, **58**, 3776–3787.

44. Lloyd, P.G., Yang, H.T. and Terjung, R.L. (2001) Arteriogenesis and angiogenesis in rat ischemic hindlimb: role of nitric oxide. *Am. J. Physiol. Heart Circ. Physiol.*, **281**, H2528–H2538.

45. Wehling, M., Spencer, M.J. and Tidball, J.G. (2001) A nitric oxide synthase transgene ameliorates muscular dystrophy in *mdx* mice. *J. Cell Biol.*, **155**, 123–131.

46. Ito, K., Kimura, S., Ozasa, S., Matsukura, M., Ikezawa, M., Yoshioka, K., Ueno, H., Suzuki, M., Araki, K., Yamamura, K., Miwa, T., Dickson, G., Thomas, G.D. and Miike, T. (2006) Smooth muscle-specific dystrophin expression improves aberrant vasoregulation in *mdx* mice. *Hum. Mol. Genet.*, **15**, 2266–2275.

47. Guggilam, A., Patel, K.P., Haque, M., Ebenezer, P.J., Kapusta, D.R. and Francis, J. (2008) Cytokine blockade attenuates sympathoexcitation in heart failure: Cross-talk between nNOS, AT-1R and cytokines in the hypothalamic paraventricular nucleus. *Eur. J. Heart Fail.*, **10**, 625–634.

48. Ehlermann, P., Eggers, K., Bierhaus, A., Most, P., Weichenhan, D., Greten, J., Nawroth, P.P., Katus, H.A. and Remppis, A. (2006) Increased proinflammatory endothelial response to S100A8/A9 after preactivation through advanced glycation end products. *Cardiovasc. Diabetol.*, **5**:6.

49. Lange, M., Nakano, Y., Traber, D.L., Hamahata, A., Esechie, A., Jonkam, C., Bansal, K., Traber, L.D. and Enkhbaatar, P. (2010) Role of different nitric oxide synthase isoforms in a murine model of acute lung injury and sepsis. *Biochem. Biophys. Res. Commun.*, **399**, 286–291.

50. Gebhardt, C., Nemeth, J., Angel, P. and Hess, J. (2006) S100A8 and S100A9 in inflammation and cancer. *Biochem. Pharmacol.*, **72**, 1622–1631.

51. Nauck, M., Karakiulakis, G., Perruchoud, A.P., Papakonstaninou, E. and Roth, M. (1998) Corticosteroid inhibit the expression of the vascular endothelial growth factor gene in human vascular smooth muscle cells. *Eur. J. Pharmacol.*, **341**, 309–315.

52. Pross, C., Farooq, M.M., Angle, N., Lane, J.S., Cerveira, J.J., Xavier, A.E., Freischlag, J.A., Law, R.E. and Gelabert, H.A. (2002) Dexamethasone inhibits vascular smooth muscle cell migration via modulation of matrix metalloproteinase activity. *J. Surg. Res.*, **102**, 57–62.

53. Menezes, L.G., Sobreira, C., Neder, L., Rodrigeus, A.L. Jr. and Martinez, J.A.B. (2007) Creatine supplementation attenuates corticosteroid-induced muscle wasting and impairment of exercise performance in rats. *J. Appl. Physiol.*, **102**, 698–703.

54. Barel, M., Perez, O.A.B., Giozzet, V.A., Rafacho, A., Bosqueiro, J.R. and Amaral, S.L. (2010) Exercise training prevents hyperinsulinemia, muscular glycogen loss and muscle atrophy induced by dexamethasone treatment. *Eur. J. Appl. Physiol.*, **108**, 999–1007.

55. Amalfitano, A. and Chamberlain, J.S. (1996) The *mdx*-amplification-resistant mutation system assay, a simple and rapid polymerase chain reaction-based detection of the *mdx* allele. *Muscle Nerve*, **19**, 1549–1553.

56. Massa, R., Silvestri, G., Zeng, Y.C., Martorana, A., Sancesario, G. and Bernardi, G. (1997) Muscle regeneration in *mdx* mice: resistance to repeated necrosis is compatible with myofiber maturity. *Basic Appl. Myol.*, **7**, 387–394.

57. Gosselin, L.E., Williams, J.E., Personius, K. and Farkas, G.A. (2007) A comparison of factors associated with collagen metabolism in different skeletal muscles from dystrophic (*mdx*) mice: impact of pirfenidone. *Muscle Nerve*, **35**, 208–216.

Legends to Figures

Figure 1

Histopathological characterization of the skeletal muscle of *mdx*/MMP-2$^{-/-}$ mice. (**A**) Hematoxylin and eosin staining of tibialis anterior (TA) muscles in *mdx* and *mdx*/MMP-2$^{-/-}$ mice at 1, 2, and 3 months of age. Scale bar: 100 μm. (**B**) The fiber size in TA muscle at 3 months of age (n = 3 for each group). Bar: mean ± S.E.M.; * $P < 0.05$, significantly different from wild-type; $^{\#\#}P < 0.01$, significantly different from MMP-2 ablation alone. (**C**) Comparison of perinuclear fibers and centronuclear regenerated fibers in TA muscle at 3 months of age (n = 3 for each group). Bar: mean ± S.E.M.; $^{\#}P < 0.05$, $^{\#\#}P < 0.01$, significantly different from MMP-2 ablation alone. (**D**) Distribution of fiber size of TA muscle in wild-type and MMP-2$^{-/-}$ mice at 3 months of age. Bar: mean ± S.E.M. (**E**) Distribution of fiber size of TA muscle in *mdx* and *mdx*/MMP-2$^{-/-}$ mice at 3 months of age. Bar: mean ± S.E.M.; $^{\#\#}P < 0.01$, significantly different from MMP-2 ablation alone.

Figure 2

Evaluation of angiogenesis in the skeletal muscle of *mdx*/MMP-2$^{-/-}$ mice. (**A**) Immunohistochemistry with PECAM-1, an epithelial marker, in TA muscle at 1 and 3 months of age. Scale bar: 100 μm. (**B**) Mean vessel size in TA muscle of *mdx*/MMP-2$^{-/-}$ mice at 1 and 3 months of age (n = 3 for each group). Bar: mean ± S.E.M.; $^{\#}P < 0.05$, significantly different from MMP-2 ablation alone. (**C**) Number of vessels per square millimeter in TA muscle at 1 and 3 months of age (n = 3 for each group). Bar: mean ±

S.E.M. (**D**) Number of vessels per myofiber in TA muscle at 1 and 3 months of age (n = 3 for each group). Bar: mean ± S.E.M.; * $P < 0.05$, significantly different from wild-type; $^{\#\#}$ $P < 0.01$, significantly different from MMP-2 ablation alone. (**E**) Endothelial area in TA muscle of *mdx*/MMP-$2^{-/-}$ mice at 1 and 3 months of age (n = 3 for each group). Bar: mean ± S.E.M.; * $P < 0.05$, significantly different from wild-type; $^{\#\#}$ $P < 0.01$, significantly different from MMP-2 ablation alone.

Figure 3

mRNA levels of various angiogenesis-related factors in *mdx*/MMP-$2^{-/-}$ mice skeletal muscle. Relative (to 18S rRNA) mRNA levels of angiopoietin-1 (**A**), angiopoietin-2 (**B**), platelet-derived growth factor (PDGF) (**C**), fibroblast growth factor (FGF) (**D**), transforming growth factor (TGF-β) (**E**), vascular endothelial growth factor (VEGF) (**F**), and VEGF receptor-1 (Flt-1) (**G**) and -2 (Flk-1) (**H**) in the skeletal muscle of wild-type, MMP-$2^{-/-}$, *mdx*, and *mdx*/MMP-$2^{-/-}$ mice at 1 and 3 months of age (n = 3 for each group). Bar: mean ± S.E.M.; * $P < 0.05$, ** $P < 0.01$, significantly different from wild-type; $^{\#}$ $P < 0.05$, $^{\#\#}$ $P < 0.01$, significantly different from MMP-2 ablation alone.

Figure 4

VEGF and its receptors protein levels and localization in the skeletal muscle of *mdx*/MMP-$2^{-/-}$. (**A**) Western blot analysis of VEGF (upper band) and internal control GAPDH (lower band) in wild-type, MMP-$2^{-/-}$, *mdx*, and *mdx*/MMP-$2^{-/-}$ mice at 1 and 3 months of age. (**B**) Relative (to GAPDH) VEGF protein levels in wild-type, MMP-$2^{-/-}$, *mdx*,

and *mdx*/MMP-2$^{-/-}$ mice at 1 and 3 months of age (n = 3 for each group). Bar: mean ± S.E.M.; * $P < 0.05$, ** $P < 0.01$, significantly different from wild-type; $^{\#\#}P < 0.01$, significantly different from MMP-2 ablation alone. (**C**) Immunohistochemistry of VEGF (red)/NCAM (green) (upper panel), Flt-1 (red)/NCAM (green) (middle panel), and Flk-1 (red)/PECAM-1 (green) (lower panel) in the skeletal muscle of wild-type, MMP-2$^{-/-}$, *mdx*, and *mdx*/MMP-2$^{-/-}$ mice at 1 and 3 months of age. Scale bar: 100 μm.

Figure 5

Nitric oxide synthase (NOS) isoform expression in the skeletal muscle of *mdx*/MMP-2$^{-/-}$ mice. Relative (to 18S rRNA) mRNA levels of nNOS (**A**), endothelial NOS (eNOS) (**B**), and inducible NOS (iNOS) (**C**) in the skeletal muscle of wild-type, MMP-2$^{-/-}$, *mdx*, and *mdx*/MMP-2$^{-/-}$ mice (n = 3 for each group). Bar: mean ± S.E.M.; ** $P < 0.01$, significantly different from wild-type; $^{\#}P < 0.05$, $^{\#\#}P < 0.01$, significantly different from MMP-2 ablation alone. (**D**) Western blot analysis of nNOS and (**E**) relative (to GAPDH) nNOS protein levels in the skeletal muscle of wild-type, MMP-2$^{-/-}$, *mdx*, and *mdx*/MMP-2$^{-/-}$ mice (n = 3 for each group). Bar: mean ± S.E.M.; * $P < 0.05$, ** $P < 0.01$, significantly different from wild-type; $^{\#}P < 0.05$, significantly different from MMP-2 ablation alone. (**F**) Immunohistochemistry of nNOS and laminin α2 in the skeletal muscle of wild-type, MMP-2$^{-/-}$, *mdx*, and *mdx*/MMP-2$^{-/-}$ mice. Scale bar: 100 μm.

Figure 6

β-dystroglycan (β-DG) degradation in *mdx*/MMP-2$^{-/-}$ mice skeletal muscle. (**A**) Western

blot analyses of β-DG in the skeletal muscle of wild-type, MMP-$2^{-/-}$, *mdx*, and *mdx*/MMP-$2^{-/-}$ mice. Full-length β-DG (βDG_{43}, upper bands) and degraded 30-kDa proteins (βDG_{30}, lower bands) were observed in both *mdx* or *mdx*/MMP-$2^{-/-}$ mice at 1 and 3 months of age. Relative (to GAPDH) levels of βDG_{43} (**B**) and βDG_{30} (**C**) revealed an increase in βDG_{43} and a decrease in βDG_{30} in *mdx*/MMP-$2^{-/-}$ compared to *mdx* at 1 month of age. Bar: mean ± S.E.M.; * $P < 0.05$, ** $P < 0.01$, significantly different from wild-type; $^{\#}P < 0.05$, $^{\#\#}P < 0.01$, significantly different from MMP-2 ablation alone.

Figure 7

Hypothetical schema of the role of MMP-2 in dystrophin-deficient skeletal muscle. We hypothesize that MMP-2 influences angiogenesis and muscle regeneration via up-regulation of VEGF and its receptor Flt-1 during regeneration of dystrophin-deficient skeletal muscle. MMP-2 may also affect angiogenesis in dystrophin-deficient skeletal muscle through coordination of NO produced by nNOS.

Supplemental Figure 1

The mRNA levels of MMP-2, -9, and -3 and tissue inhibitor of metalloproteinase (TIMP)-1 and -2 determined by real-time PCR; the protein activity of MMP-2 and -9 determined by gelatin zymography; protein levels of MMP-9 determined by western blotting in the skeletal muscle of *mdx*/MMP-$2^{-/-}$ mice. Relative (to 18S rRNA) mRNA levels of MMP-2 (A) and MMP-9 (B) in the skeletal muscle of wild-type, MMP-$2^{-/-}$, *mdx*, and *mdx*/MMP-$2^{-/-}$ mice at 1 and 3 months of age (n = 3 for each group). MMP-2 and -9 protein activity

determined by gelatin zymography in the skeletal muscle of wild-type, MMP-2$^{-/-}$, *mdx*, and *mdx*/MMP-2$^{-/-}$ mice at 1 and 3 months of age (C). Myosin heavy chain (MHC) was used as the loading control. Western blot analysis of MMP-9 (D) and relative (to GAPDH) pro-MMP-9 (E) and active-MMP-9 (F) protein levels in the skeletal muscle of the wild-type, MMP-2$^{-/-}$, *mdx*, and *mdx*/MMP-2$^{-/-}$ mice (n = 3 for each group). Relative (to 18S rRNA) mRNA levels of MMP-3 (G), TIMP-1 (H), and TIMP-2 (I) in the skeletal muscle of the wild-type, MMP-2$^{-/-}$, *mdx*, and *mdx*/MMP-2$^{-/-}$ mice at 1 and 3 months of age (n = 3 for each group). Bar: mean ± SEM; * $P < 0.05$, ** $P < 0.01$, significantly different from wild-type; $^{\#}$ $P < 0.05$, $^{\#\#}$ $P < 0.01$, significantly different from MMP-2 ablation alone.

Supplemental Figure 2

Clinical and pathological characterization of *mdx*/MMP-2$^{-/-}$ mice. Body weight at 1 and 3 months of age (**A**), and hanging wire test (**B**) and serum CK levels (**C**) at 3 months of age, in wild-type, MMP-2$^{-/-}$, *mdx*, and *mdx*/MMP-2$^{-/-}$ mice (n = 3 for each group). Bar shows mean ± S.E.M. (**D**) ATPase (pH 9.4) staining of TA of wild-type, MMP-2$^{-/-}$, *mdx*, and, *mdx*/MMP-2$^{-/-}$ mice at 3 months of age. Scale bar: 100 μm.

Supplemental Figure 3

Morphometric analysis of diaphragm, quadriceps, and gastrocnemius muscle sections in *mdx* and *mdx*/MMP-2$^{-/-}$ mice at 1 and 3 moths of age. H&E staining of diaphragm, quadriceps, and gastrocnemius muscles in *mdx* and *mdx*/MMP-2$^{-/-}$ mice at 1 and 3 months of age under low magnification (**A**) and at 3 months of age under high magnification (**B**).

Scale bar: 100 μm. The mean fiber size in diaphragm (**C**), quadriceps (**D**), and gastrocnemius (**E**) in *mdx* and *mdx*/MMP-2$^{-/-}$ mice at 3 months of age.

Supplemental Figure 4

Cardiotoxin-induced muscle injury in MMP-2$^{-/-}$ mice. (**A**) H&E staining of TA muscles under cardiotoxin injection in wild-type and MMP-2$^{-/-}$ mice at 6 weeks of age. Scale bar: 100 μm. (**B**) The mean fiber size in TA muscles 7 days after cardiotoxin injection in wild-type and MMP-2$^{-/-}$ at 6 weeks of age. (**C**) Distribution of TA muscle fiber size 7 days after cardiotoxin injection in wild-type and MMP-2$^{-/-}$ mice at 6 weeks of age.

Supplemental Figure 5

Localization of VEGF and Mac-3 by immunohistochemistry. Immunohistochemistry of VEGF and Mac-3, a marker of macrophages, in the skeletal muscle of wild-type, MMP-2$^{-/-}$, *mdx*, and *mdx*/MMP-2$^{-/-}$ mice at 1 and 3 months of age. Scale bar: 100 μm.

Supplemental Figure 6

mRNA levels of various myogenic and growth factors in *mdx*/MMP-2$^{-/-}$ mice skeletal muscle. Relative (to 18S rRNA) mRNA levels of pax-3 (**A**), pax-7 (**B**), MyoD (**C**), Myf-5 (**D**), myogenin (**E**), MEF2a (**F**), insulin-like growth factor (IGF) (**G**), myostatin (**H**), and follistatin (**I**) in the skeletal muscle of wild-type, MMP-2$^{-/-}$, *mdx*, and *mdx*/MMP-2$^{-/-}$ mice at 1 and 3 months of age (n = 3 for each group). Bar: mean ± S.E.M.; * $P < 0.05$, ** $P < 0.01$, significantly different from wild-type.

Supplemental Figure 7

Differentially expressed genes in the microarray analysis. A scatter graph of differential gene expression analyses, using microarrays in *mdx* and *mdx*/MMP-2$^{-/-}$ mice at 1 (**A**) and 3 (**B**) months of age. The upper and lower lines show 2.0- and 0.5- fold changes in gene expression levels between the 2 groups, respectively. Relative (to 18S rRNA) levels of S100A8 (**C**), S100A9 (**D**), CCL-2 (**E**). CCL-7 (**F**), CCR-1 (**G**), CCR-2 (**H**), and chitinase 3-like 3 (**I**) in the skeletal muscle of *mdx* with MMP-2 ablation at 3 months of age (n = 3 for each group) evaluated using real-time PCR. Bar: mean ± S.E.M.; * $P < 0.05$, ** $P < 0.01$, significantly different from wild-type; $^{\#\,\#}$ $P < 0.01$, significantly different from MMP-2 ablation alone.

Supplemental Figure 8

β-Sarcoglycan expression in the skeletal muscle of *mdx*/MMP-2$^{-/-}$ mice at 1 and 3 months of age. (**A**) Western blot analysis of β-sarcoglycan and (**B**) relative (to GAPDH) β-sarcoglycan protein levels in the skeletal muscle of wild-type, MMP-2$^{-/-}$, *mdx*, and *mdx*/MMP-2$^{-/-}$ mice (n = 3 for each group). Bar: mean ± S.E.M.; * $P < 0.05$, ** $P < 0.01$, significantly different from wild-type. (**C**) Immunohistochemistry of β-sarcoglycan and laminin α2 in the skeletal muscle of wild-type, MMP-2$^{-/-}$, *mdx*, and *mdx*/MMP-2$^{-/-}$ mice. Scale bar: 100 μm.

Tables

Supplemental Table 1. Differentially up-regulated or down-regulated gene classes in mdx/MMP-$2^{-/-}$ mice

Up-regulated at 1 month of age	Number of genes (% of total)
Protein binding	2 (15.4)
Regulation of apoptosis	2 (15.4)
Myosin complex	2 (15.4)
Metal ion binding	1 (7.7)
Other	2 (15.4)
Unknown	4 (30.8)

Down-regulated at 1 month of age	Number of genes (% of total)
Protein binding	2 (11.1)
Nucleotide binding	2 (11.1)
Multicellular organismal development	2 (11.1)
Regulation of cell growth	2 (11.1)
Collagen fibril organization	2 (11.1)
Metallopeptidase activity	1 (5.6)
Cytokine and receptor	1 (5.6)
Integrin-mediated signaling pathway	1 (5.6)
Other	4 (22.2)
Unknown	1 (5.6)

Up-regulated at 3 months of age	Number of genes (% of total)
Protein binding	10 (14.5)
Signal transduction	7 (10.2)
Chemokine and receptor	6 (8.7)
Regulation of cell growth	5 (7.3)
Nucleotide binding	4 (5.8)
Immune response	4 (5.8)
Calcium ion binding	3 (4.4)
Metallopeptidase activity	3 (4.4)
Cytokine and receptor	3 (4.4)
Angiogenesis	3 (4.4)
Regulation of apoptosis	3 (4.4)
Cell adhesion	2 (2.9)
Endopeptidase inhibitor activity	2 (2.9)
Nitric oxide mediated signal transduction	2 (2.9)
Metal ion binding	1 (1.5)
Collagen fibril organization	1 (1.5)
Proteolysis	1 (1.5)
Oxidation-reduction	1 (1.5)

Integrin-mediated signaling pathway	1 (1.5)
Other	6 (8.7)
Unknown	1 (1.5)

Down-regulated at 3 months of age	Number of genes (% of total)
Nucleotide binding	4 (30.8)
Signal transduction	2 (15.4)
Protein binding	1 (7.7)
Multicellular organismal development	1 (7.7)
Angiogenesis	1 (7.7)
Other	3 (23.1)
Unknown	1 (7.7)

Supplemental Table 2. Selected genes differentially up-regulated in *mdx*/MMP-2$^{-/-}$ at 1 month of age

Gene class	RefSeq transcript ID	Gene title	Fold change
Protein binding	NM_001081390	Palladin, cytoskeletal associated protein	2.1
	NM_009172	Seven in absentia 1A (Siah1a), mRNA	2.1
Regulation of apoptosis	NM_020581	Angiopoietin-like 4	2.3
	NM_009357	Testis-expressed gene 261	2.2
Myosin complex	NM_080728	Myosin, heavy polypeptide 7, cardiac muscle, beta	2.3
	NM_010856	Myosin, heavy polypeptide 6, cardiac muscle, alpha	2.0
Metal ion binding	XM_127602	Zinc finger, MYND domain containing 17	2.2
Other	NM_022314	Tropomyosin 3, gamma	2.0
	NM_130858	Neurexophilin 3	2.0
Unknown	NM_001081402	WD repeat domain 70	2.8
	NM_030179	CAP-GLY domain containing linker protein family, member 4	2.2
	XM_901568	RNA imprinted and accumulated in nucleus	2.2
	NR_003633	Maternally expressed 3	2.1

Supplemental Table 3. Selected genes differentially down-regulated in *mdx*/MMP-2$^{-/-}$ at 1 month of age

Gene class	RefSeq transcript ID	Gene title	Fold change
Protein binding	NM_009837	Chaperonin containing Tcp1, subunit 4 (delta)	0.3
	XM_001000130	Glutamate receptor interacting protein 2	0.5
Nucleotide binding	NM_010234	FBJ osteosarcoma oncogene	0.4
	NM_008656	Myogenic factor 5	0.5
Multicellular organismal development	NM_178642	Anoctamin 1, calcium-activated chloride channel	0.4
	NM_145602	N-myc downstream-regulated gene 4	0.5
Regulation of cell growth	NM_007707	Suppressor of cytokine signaling 3	0.2
	NM_010849	Myelocytomatosis oncogene	0.5
Collagen fibril organization	NM_001113515	Collagen, type II, alpha 1	0.2
	NM_007729	Collagen, type XI, alpha 1	0.5
Metallopeptidase activity	NM_008607	Matrix metallopeptidase 13	0.3
Cytokine and receptor	NM_009778	Complement component 3	0.5
Integrin-mediated signaling pathway	NM_008318	Integrin-binding sialoprotein	0.1
Other	NM_175151	TatD DNase domain containing 1	0.3
	NM_008212	Hydroxyacyl-coenzyme A dehydrogenase	0.4
	NM_019758	Mitochondrial carrier homolog 2 (*C. elegans*)	0.4
	NM_001081116	Rho guanine nucleotide exchange factor (GEF) 17	0.5
Unknown	XM_001481283	PWWP domain containing 2A	0.4

Supplemental Table 4. Selected genes differentially up-regulated in *mdx*/MMP-2$^{-/-}$ at 3 months of age

Gene class	RefSeq transcript ID	Gene title	Fold change
Protein binding	NM_001113326	Macrophage scavenger receptor 1	2.5
	NM_177364	SH3 and PX domains 2B	2.4
	XM_001479984	Expressed sequence AI607873	2.4
	NM_007408	Adipose differentiation-related protein	2.3
	NM_001025261	Tumor protein D52	2.3
	NM_008879	Lymphocyte cytosolic protein 1	2.3
	NM_001008702	Disabled homolog 2 (*Drosophila*)	2.3
	NM_001045481	Interferon-activated gene 203	2.2
	NM_028071	Coactosin-like 1 (*Dictyostelium*)	2.2
	NM_001136055	CD82 antigen	2.2
Signal transduction	NM_029499	Membrane-spanning 4-domains, subfamily A, member 4C	3.9
	NM_026835	Membrane-spanning 4-domains, subfamily A, member 6D	3.1
	NM_001130150	Rho guanine nucleotide exchange factor (GEF) 1	2.5
	NM_019549	Pleckstrin	2.4
	NM_008013	Fibrinogen-like protein 2	2.2
	NM_028595	Membrane-spanning 4-domains, subfamily A, member 6C	2.2
	NM_027209	Membrane-spanning 4-domains, subfamily A, member 6B	2.2
Chemokine and receptor	NM_013654	Chemokine (C-C motif) ligand 7	5.1
	NM_009912	Chemokine (C-C motif) receptor 1	4.8
	NM_011333	Chemokine (C-C motif) ligand 2	3.4
	NM_011338	Chemokine (C-C motif) ligand 9	2.6
	NM_009915	Chemokine (C-C motif) receptor 2	2.5
	NM_009139	Chemokine (C-C motif) ligand 6	2.4
Regulation of cell growth	NM_009898	Coronin, actin-binding protein 1A	3.5
	NM_016873	WNT1 inducible signaling pathway protein 2	3.0
	NM_007707	Suppressor of cytokine signaling 3	2.5
	NM_001113529	Colony-stimulating factor 1 (macrophage)	2.2
	NM_013492	Clusterin	2.2
Nucleotide binding	NM_019662	Ras-related associated with diabetes	3.1

	NM_029688	Sulfiredoxin 1 homolog (*S. cerevisiae*)	2.5
	NM_172856	LAG1 homolog, ceramide synthase 6	2.5
	NM_010613	KH-type splicing regulatory protein	2.4
Immune response	NM_009892	Chitinase 3-like 3	11.9
	NM_010819	C-type lectin domain family 4, member d	2.8
	NM_020001	C-type lectin domain family 4, member n	2.6
	NM_011999	C-type lectin domain family 4, member a2	2.2
Calcium ion binding	NM_009114	S100 Calcium-binding protein A9 (calgranulin B)	11.7
	NM_013650	S100 Calcium-binding protein A8 (calgranulin A)	10.8
	NM_011311	S100 Calcium-binding protein A4	2.3
Metallopeptidase activity	NM_001044384	Tissue inhibitor of metalloproteinase 1	3.8
	NM_010809	Matrix metallopeptidase 3	3.1
	NM_008608	Matrix metallopeptidase 14 (membrane-inserted) (Mmp14)	2.3
Cytokine and receptor	NM_001077705	Protein tyrosine phosphatase, non-receptor type 6	4.5
	NM_009263	Secreted phosphoprotein 1	2.9
	NM_133990	Interleukin 13 receptor, alpha 1	2.7
Angiogenesis	NM_007585	Annexin A2	4.0
	NM_010728	Lysyl oxidase	2.3
	NM_008871	Serine (or cysteine) peptidase inhibitor, clade E, member 1	2.2
Regulation of apoptosis	NM_019980	LPS-induced TN factor	2.9
	NM_172422	FAST kinase domains 2	2.7
	NM_007987	Fas (TNF receptor superfamily member 6)	2.6
Cell adhesion	NM_139200	Cytohesin 1-interacting protein	2.7
	NM_145158	Elastin microfibril interface 2	2.5
Endopeptidase inhibitor activity	NM_009252	Serine (or cysteine) peptidase inhibitor, clade A, member 3N	2.7
	NM_025429	Serine (or cysteine) peptidase inhibitor, clade B, member 1a	2.3
Nitric oxide-mediated signal transduction	NM_013602	Metallothionein 1	2.6
	NM_008630	Metallothionein 2	2.5
Metal ion binding	NM_134152	Leupaxin	2.4
Collagen fibril organization	NM_007739	Collagen, type VIII, alpha 1	2.8
Proteolysis	NM_017370	Haptoglobin	3.3
Oxidation-reduction	NM_010271	Glycerol-3-phosphate dehydrogenase 1 (soluble)	3.3
Integrin-mediated signaling pathway	NM_007403	A disintegrin and metallopeptidase domain 8	2.4

Other	NM_011410	Schlafen 4	6.5
	NM_001083917	Sodium channel, voltage-gated, type III, beta	2.9
	NM_011216	Protein tyrosine phosphatase, receptor type, O	2.6
	NM_011671	Uncoupling protein 2 (mitochondrial, proton carrier)	2.4
	NM_001135151	Solute carrier family 39 (zinc transporter), member 14	2.3
	NM_029512	Tocopherol (alpha) transfer protein-like	2.2
Unknown	NM_001110146	Proteoglycan 4 (megakaryocyte-stimulating factor)	2.3

Supplemental Table 5. Selected genes differentially down-regulated in *mdx*/MMP-2$^{-/-}$ at 3 months of age

Gene class	RefSeq transcript ID	Gene title	Fold change
Nucleotide binding	NM_015743	Nuclear receptor subfamily 4, group A, member 3	0.3
	NM_027236	Eukaryotic translation initiation factor 1A domain containing	0.5
	NM_013914	Snail homolog 3 (Drosophila)	0.5
	NM_144812	Trinucleotide repeat containing 6b	0.5
Signal transduction	NM_175535	Rho GTPase activating protein 20	0.4
	NM_001122759	Phosphodiesterase 7A	0.4
Protein binding	NM_019765	CAP-GLY domain containing linker protein 1	0.5
Multicellular organismal development	NM_145602	N-myc downstream regulated gene 4	0.5
Angiogenesis	NM_178444	EGF-like domain 7	0.5
Other	NM_001103177	Actin-binding LIM protein 1	0.3
	NM_008059	G0/G1 switch gene 2	0.5
	NM_013635	Synaptophysin-like protein	0.5
Unknown	NM_197986	Transmembrane protein 140	0.5

Supplemental Table 6. Primers used for the real-time PCR analysis

18S ribosomal RNA	Forward	5'–ATCATGCAGAACCCACGACA–3'
(18S rRNA)	Reverse	5'–ACACGAAGGCCCCAAAAGT–3'
Angiopoietin-1	Forward	5'–AACACCAACGCTCTGCAAAG–3'
(Ang-1)	Reverse	5'–CCGTGTGGTTTTGAACAGCA–3'
Angiopoietin-2	Forward	5'–TGCAAGTGTTCCCAGATGCT–3'
(Ang-2)	Reverse	5'–TGGTAGTGTAGGCAGGCATT–3'
Platelet-driving growth factor	Forward	5'–TTGAACATGACCCGAGCACA–3'
(PDGF)	Reverse	5'–TTGGTGCGATCGATGAGGTT–3'
Transforming growth factor β	Forward	5'–AAGACTTCACCCCAAAGCTG–3'
(TGF-β)	Reverse	5'–AGCGCTCTCTGAGATCCAAA–3'
Fibroblast growth factor	Forward	5'–TGCAAGTTCCGAGAAACCCT–3'
(FGF)	Reverse	5'–CAGAAAAGACGCAGCTGTCA–3'
Vascular endothelial growth factor-A	Forward	5'–TGCGGATCAAACCTCACCAA–3'
(VEGF-A)	Reverse	5'–TGTTCTGTCAACGGTGACGA–3'
FMS-related tyrosine kinase 1	Forward	5'–TGCTGGGCATAAAGCAGTCA–3'
(Flt-1/VEGFR-1)	Reverse	5'–ATGCCATACACGGTGCAAGT–3'
Fetal liver kinase 1	Forward	5'–TCCGAGTTCACACAAAGCCT–3'
(Flk-1/VEGF-2)	Reverse	5'–TGGTGAGTTCATCGCCAACA–3'
Neuronal nitric oxide synthase	Forward	5'–ATGGCAAGCATGACTTCCGA–3'
(nNOS)	Reverse	5'–AGAGTTCAGGGTCATTGCCA–3'
Endothelial nitric oxide synthase	Forward	5'–CGTTCAGCCATCACAGTGTT–3'
(eNOS)	Reverse	5'–CACATCAAAGCGGCCATTTC–3'
Inducible nitric oxide synthase	Forward	5'–TCACTGGGACAGCACAGAAT–3'
(iNOS)	Reverse	5'–GAAATCCGATGTGGCCTTGT–3'
Paired box gene 3	Forward	5'–TTACCGCTGAAGAGGAAGCA–3'
(pax-3)	Reverse	5'–TTGGCTCCAGCTTGTTTCCT–3'

Paired box gene 7	Forward	5'–TTCCTGTGGAAACGGGACAA–3'
(pax-7)	Reverse	5'–AGATGGCACACTGGTTTTCC–3'
Myogenic differentiation 1	Forward	5'–TCGACTGCCTGTCCAGCAT–3'
(MyoD)	Reverse	5'–TTGAGCCTGCAGGACACTGA–3'
Myogenic factor 5	Forward	5'–TTGTGGATCGGATCACGTCT–3'
(Myf5)	Reverse	5'–ACGTATTCTGCCCAGCTTGT–3'
Myogenin	Forward	5'–AGTGGGGCAATGCACTGGA–3'
	Reverse	5'–TGGTTTCGTCTGGGAAGGCA–3'
Myocyte-specific enhancer factor 2A	Forward	5'–TGGCAGCCAGCTCAACATTA–3'
(MEF 2a)	Reverse	5'–ATTTGGAGAGGCCCTTGAGT–3'
Insulin-like growth factor	Forward	5'–TCAGTTCGTGTGTGGACCGA–3'
(IGF)	Reverse	5'–GCTCCGGAAGCAACACTCAT–3'
Myostatin	Forward	5'–ACTTTGGGCTTGACTGCGAT–3'
	Reverse	5'–GGTTTGCTTGGTGCACAAGA–3'
Follistatin	Forward	5'–AACGTGTGAGAACGTGGACT–3'
	Reverse	5'–TTTGCATCTGGCCTTGAGGA–3'
Matrix metalloproteinase-2	Forward	5'–CAACGATGGAGGCACGAGTG–3'
(MMP-2)	Reverse	5'–TGGGGCAGCCATAGAAAGTGT–3'
Matrix metalloproteinase-9 *	Forward	5'–TCCTACTCTGCCTGCACCACTAAAG–3'
(MMP-9)	Reverse	5'–CTGTACCCTTGGTCTGGACAGAAAC–3'
Matrix metalloproteinase-3	Forward	5'–AACAGTCTTGGCTCATGCCT–3'
(MMP-3)	Reverse	5'–AGTGGCCAAGTTCATGAGCA–3'
Tissue inhibitor of metalloproteinase-1	Forward	5'–TGTGGGAAATGCCGCAGATA–3
(TIMP-1)	Reverse	5'–GCAGGCACTGATGTGCAAAT–3
Tissue inhibitor of metalloproteinase-2	Forward	5'–ACGCTTAGCATCACCCAGAA–3
(TIMP-2)	Reverse	5'–TGGTGCCCATTGATGCTCTT–3
S100 Calcium-binding protein A8	Forward	5'–GTGTCCTCAGTTTGTGCAGA–3'
(S100A8)	Reverse	5'–ACTCCTTGTGGCTGTCTTTG–3'

S100 Calcium-binding protein A9	Forward	5'–GGACACAAACCAGGACAATC–3'
(S100A9)	Reverse	5'–GTCACATGGCTGACCTCTTA–3'
Chemokine C-C motif ligand 2	Forward	5'–AACTGCATCTGCCCTAAGGT–3'
(CCL-2)	Reverse	5'–TCACTGTCACACTGGTCACT–3'
Chemokine C-C motif ligand 7	Forward	5'–TTCCTCACCGCTGTTCTTTC–3'
(CCL-7)	Reverse	5'–ACATGAGGTCTCCAGAGCTT–3'
Chemokine C-C motif receptor 1	Forward	5'–AGGCATGTGGCTATACCACT–3'
(CCR-1)	Reverse	5'–ACCTTCCTTGGTTGACACCT–3'
Chemokine C-C motif receptor 2	Forward	5'–CCTCTTTGCCTTGTGGCAAT–3'
(CCR-2)	Reverse	5'–AGAGCCCTGCTCACTTTCAT–3'
Chitinase 3-like 3	Forward	5'–AGGATGGCTACACTGGAGAA–3'
	Reverse	5'–GGTATGCCCATATGCTGGAA–3'

* referenced by a previous report (57)

Abbreviations

Ang-1, angiopoietin-1

Ang-2, angiopoietin-2

ANOVA, analysis of variance

CCL, chemokine C-C motif ligand

CCR, chemokine C-C motif receptor

CSA, cross-sectional area

DAPI, 4',6-diamino-2-phenylindole

DG, dystroglycan

DGC, dystrophin-glycoprotein complex

DMD, Duchenne muscular dystrophy

DNA, deoxyribonucleic acid

ECM, extracellular matrix

eNOS, endothelial nitric oxide synthase

FGF, fibroblast growth factor

Flk-1, Fetal liver kinase 1

Flt-1, FMS-related tyrosine kinase 1

GAPDH, glyceraldehyde-3-phosphate dehydrogenase

H&E, hematoxylin and eosin

IGF, insulin-like growth factor

iNOS, inducible nitric oxide synthase

MEF 2a, Myocyte-specific enhancer factor 2A

MMP, matrix metalloproteases

mRNA, messenger RNA

Myf5, myogenic factor 5

MyoD, myogenic differentiation 1

NCAM, neural cell adhesion molecule

nNOS, neuronal nitric oxide synthase

NO, nitric oxide

NOS, nitric oxide synthase

pax, paired box gene

PBS, phosphate-buffered saline

PDGF, platelet-derived growth factor

RNA, ribonucleic acid

rRNA, ribosomal RNA

RT-PCR, real-time polymerase chain reaction

S100, S100 calcium-binding protein

S.E.M., standard error on the mean

TA, tibialis anterior

TBST, Tris-buffer, 0.1% Tween 20

TGF-β, transforming growth factor-β

TIMP, tissue inhibitor of metalloproteinase

VEGF-A, vascular endothelial growth factor-A

Figure 1

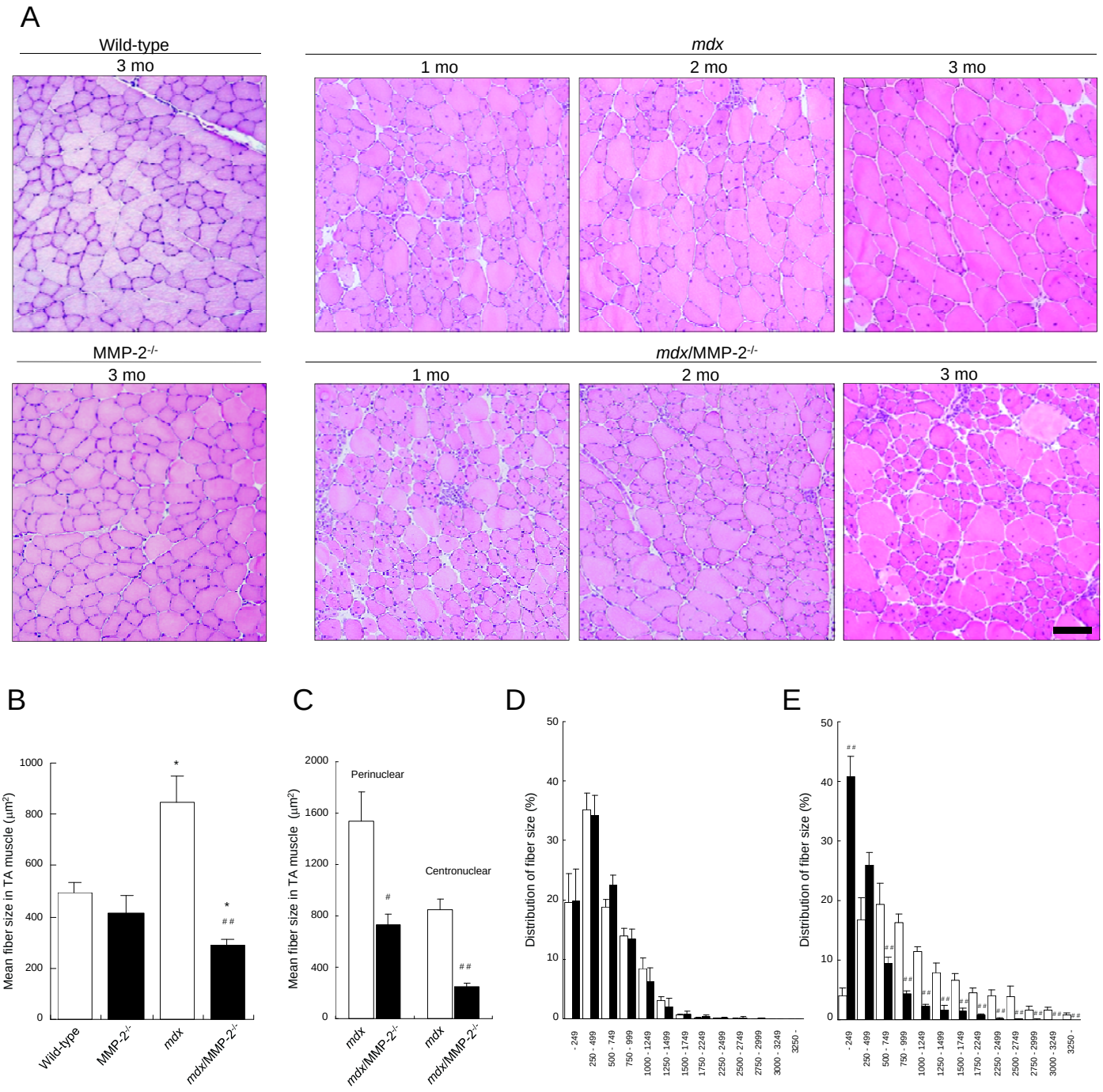
A
Wild-type
3 mo
mdx
1 mo
2 mo
3 mo
MMP-2-/-
3 mo
mdx/MMP-2-/-
1 mo
2 mo
3 mo
B
Mean fiber size in TA muscle (μm2)
1000
800
600
400
200
0
*
*
##
Wild-type
MMP-2-/-
mdx
mdx/MMP-2-/-
C
Mean fiber size in TA muscle (μm2)
2000
1600
1200
800
400
0
Perinuclear
Centronuclear
#
##
mdx
mdx/MMP-2-/-
mdx
mdx/MMP-2-/-
D
Distribution of fiber size (%)
50
40
30
20
10
0
- 249
250 - 499
500 - 749
750 - 999
1000 - 1249
1250 - 1499
1500 - 1749
1750 - 2249
2250 - 2499
2500 - 2749
2750 - 2999
3000 - 3249
3250 -
E
Distribution of fiber size (%)
50
40
30
20
10
0
##
- 249
250 - 499
500 - 749
750 - 999
1000 - 1249
1250 - 1499
1500 - 1749
1750 - 2249
2250 - 2499
2500 - 2749
2750 - 2999
3000 - 3249
3250 -

Figure 2

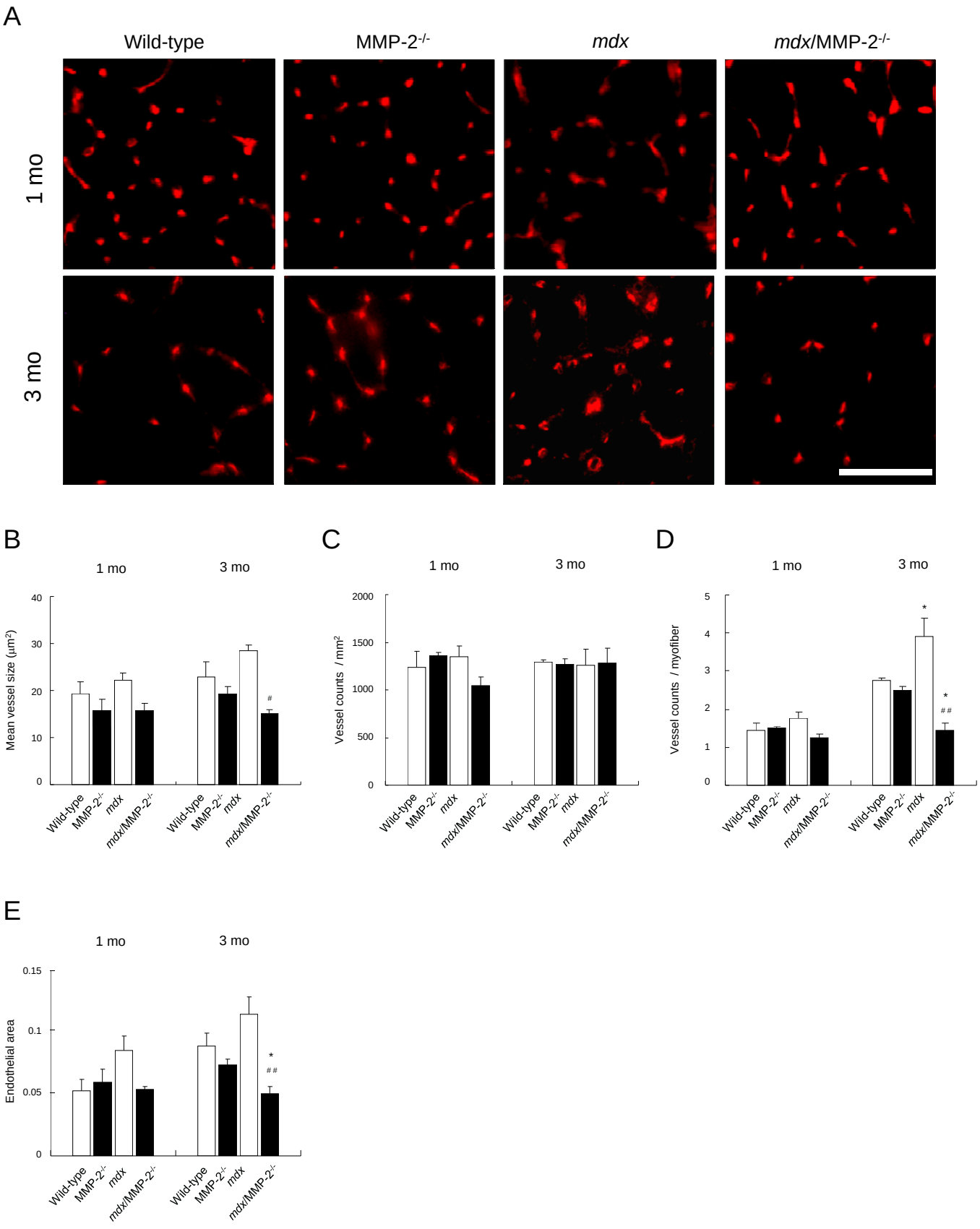
A
Wild-type
MMP-2-/-
mdx
mdx/MMP-2-/-
1 mo
3 mo
B
1 mo
3 mo
Mean vessel size (μm2)
40
30
20
10
0
#
Wild-type
MMP-2-/-
mdx
mdx/MMP-2-/-
C
1 mo
3 mo
Vessel counts / mm2
2000
1500
1000
500
0
D
1 mo
3 mo
Vessel counts / myofiber
5
4
3
2
1
0
*
*
##
E
1 mo
3 mo
Endothelial area
0.15
0.1
0.05
0
*
##

Figure 3

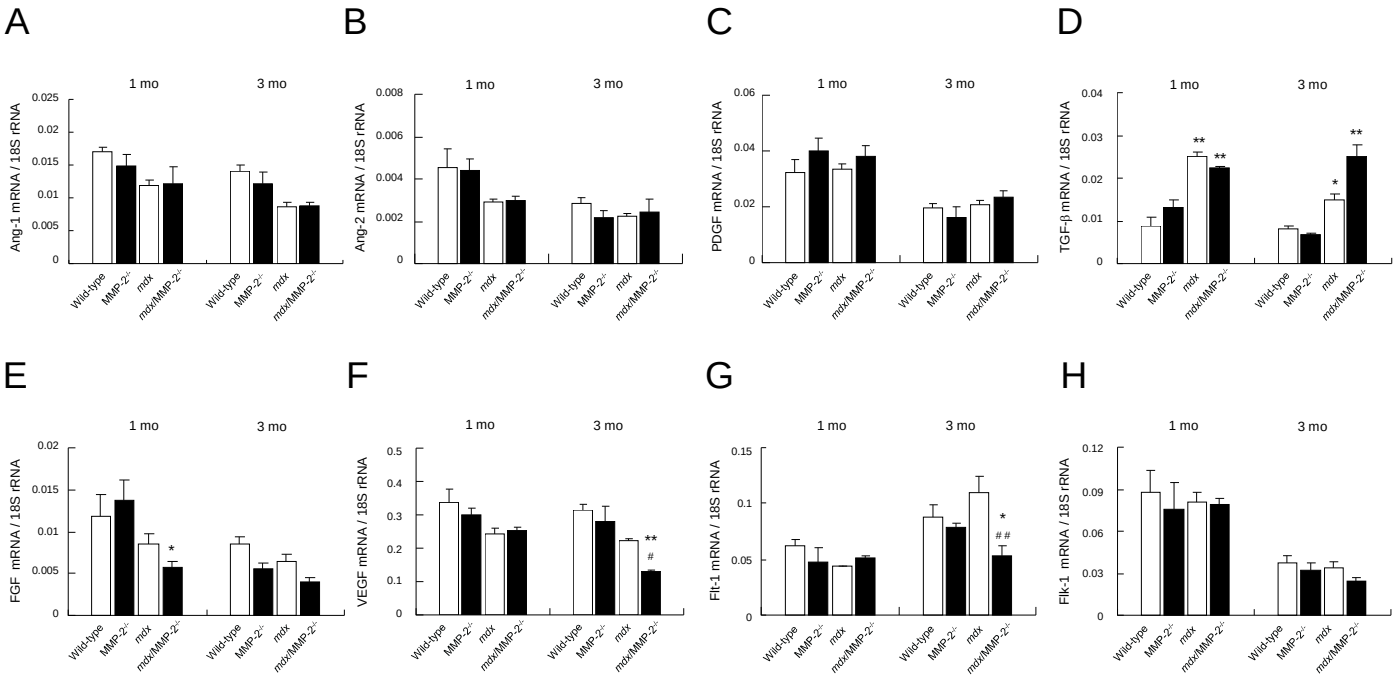
A
B
C
D
E
F
G
H
1 mo
3 mo
Ang-1 mRNA / 18S rRNA
Ang-2 mRNA / 18S rRNA
PDGF mRNA / 18S rRNA
TGF-β mRNA / 18S rRNA
FGF mRNA / 18S rRNA
VEGF mRNA / 18S rRNA
Flt-1 mRNA / 18S rRNA
Flk-1 mRNA / 18S rRNA
Wild-type
MMP-2-/-
mdx
mdx/MMP-2-/-

Figure 4

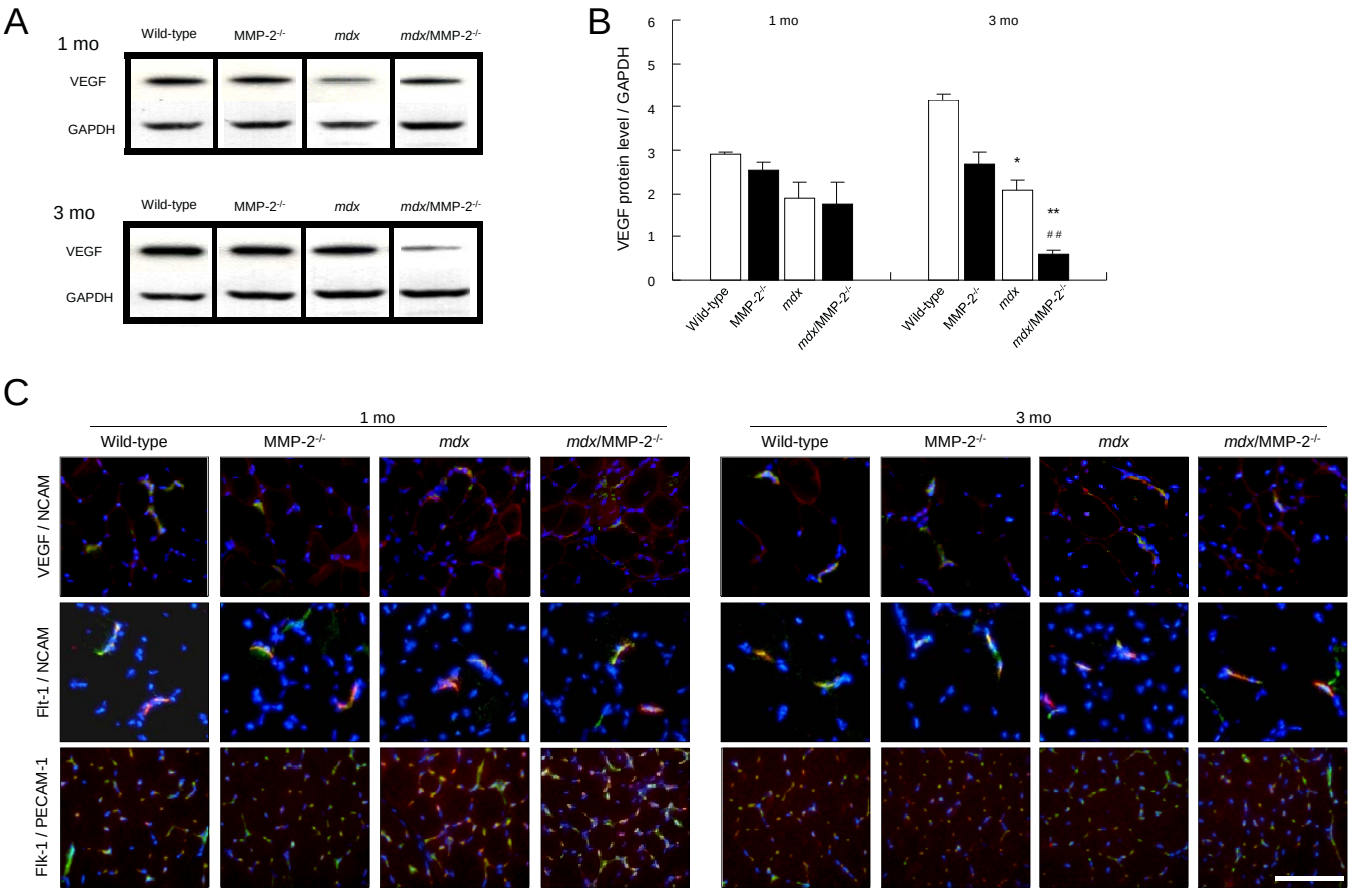
A
1 mo
Wild-type
MMP-2-/-
mdx
mdx/MMP-2-/-
VEGF
GAPDH
3 mo
Wild-type
MMP-2-/-
mdx
mdx/MMP-2-/-
VEGF
GAPDH
B
1 mo
3 mo
VEGF protein level / GAPDH
0
1
2
3
4
5
6
*
**
##
Wild-type
MMP-2-/-
mdx
mdx/MMP-2-/-
Wild-type
MMP-2-/-
mdx
mdx/MMP-2-/-
C
1 mo
3 mo
Wild-type
MMP-2-/-
mdx
mdx/MMP-2-/-
Wild-type
MMP-2-/-
mdx
mdx/MMP-2-/-
VEGF / NCAM
Flt-1 / NCAM
Flk-1 / PECAM-1

Figure 5

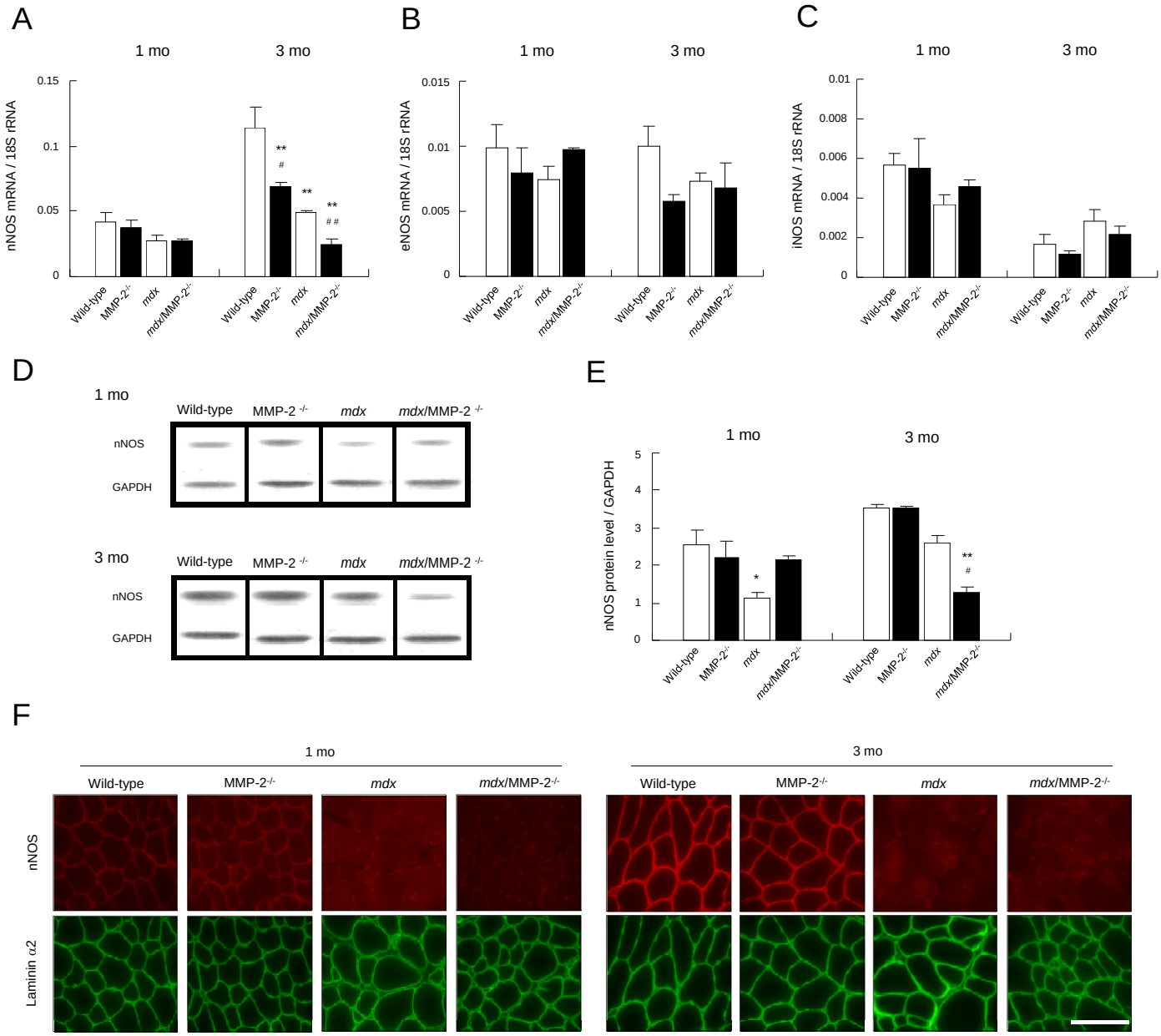
A
1 mo
3 mo
nNOS mRNA / 18S rRNA
0.15
0.1
0.05
0
**
#
**
**
##
Wild-type
MMP-2-/-
mdx
mdx/MMP-2-/-
B
1 mo
3 mo
eNOS mRNA / 18S rRNA
0.015
0.01
0.005
0
Wild-type
MMP-2-/-
mdx
mdx/MMP-2-/-
C
1 mo
3 mo
iNOS mRNA / 18S rRNA
0.01
0.008
0.006
0.004
0.002
0
Wild-type
MMP-2-/-
mdx
mdx/MMP-2-/-
D
1 mo
Wild-type
MMP-2 -/-
mdx
mdx/MMP-2 -/-
nNOS
GAPDH
3 mo
Wild-type
MMP-2 -/-
mdx
mdx/MMP-2 -/-
nNOS
GAPDH
E
1 mo
3 mo
nNOS protein level / GAPDH
5
4
3
2
1
0
*
**
#
Wild-type
MMP-2-/-
mdx
mdx/MMP-2-/-
F
1 mo
3 mo
Wild-type
MMP-2-/-
mdx
mdx/MMP-2-/-
nNOS
Laminin α2

Figure 6

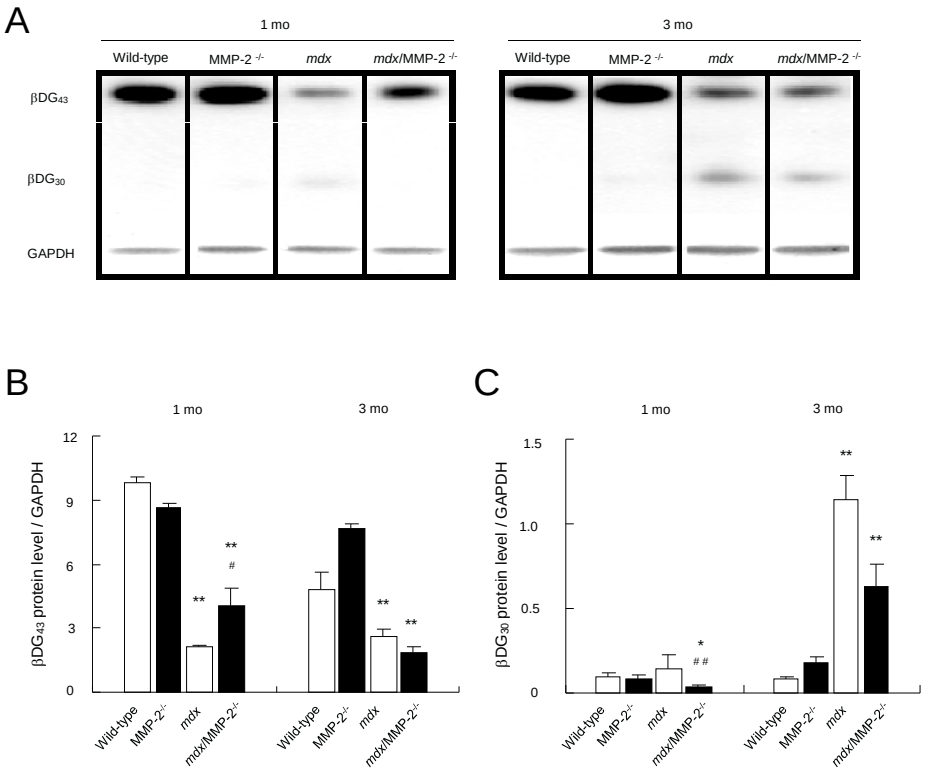
A
1 mo
3 mo
Wild-type
MMP-2 -/-
mdx
mdx/MMP-2 -/-
βDG43
βDG30
GAPDH
B
1 mo
3 mo
βDG43 protein level / GAPDH
12
9
6
3
0
**
#
C
βDG30 protein level / GAPDH
1.5
1.0
0.5
0
*
##

Figure 7

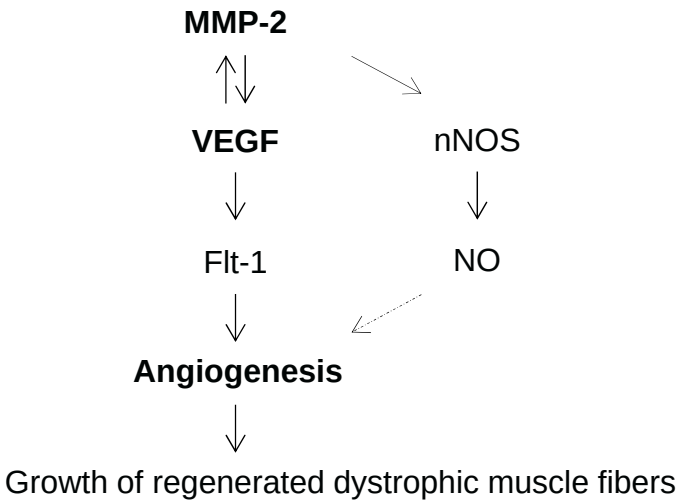
MMP-2
VEGF
nNOS
Flt-1
NO
Angiogenesis
Growth of regenerated dystrophic muscle fibers

Supplemental Figure 1

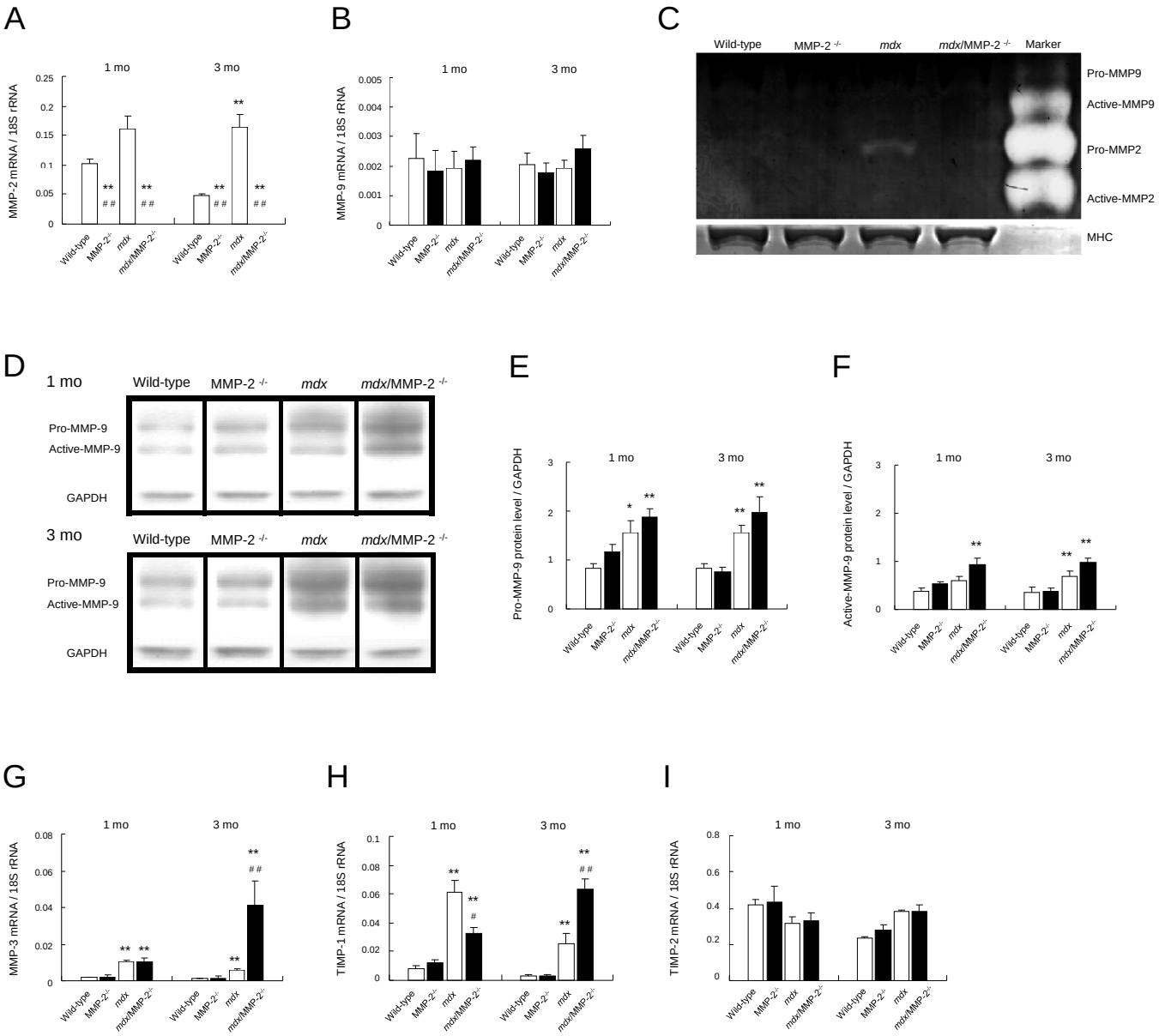

Supplemental Figure 2

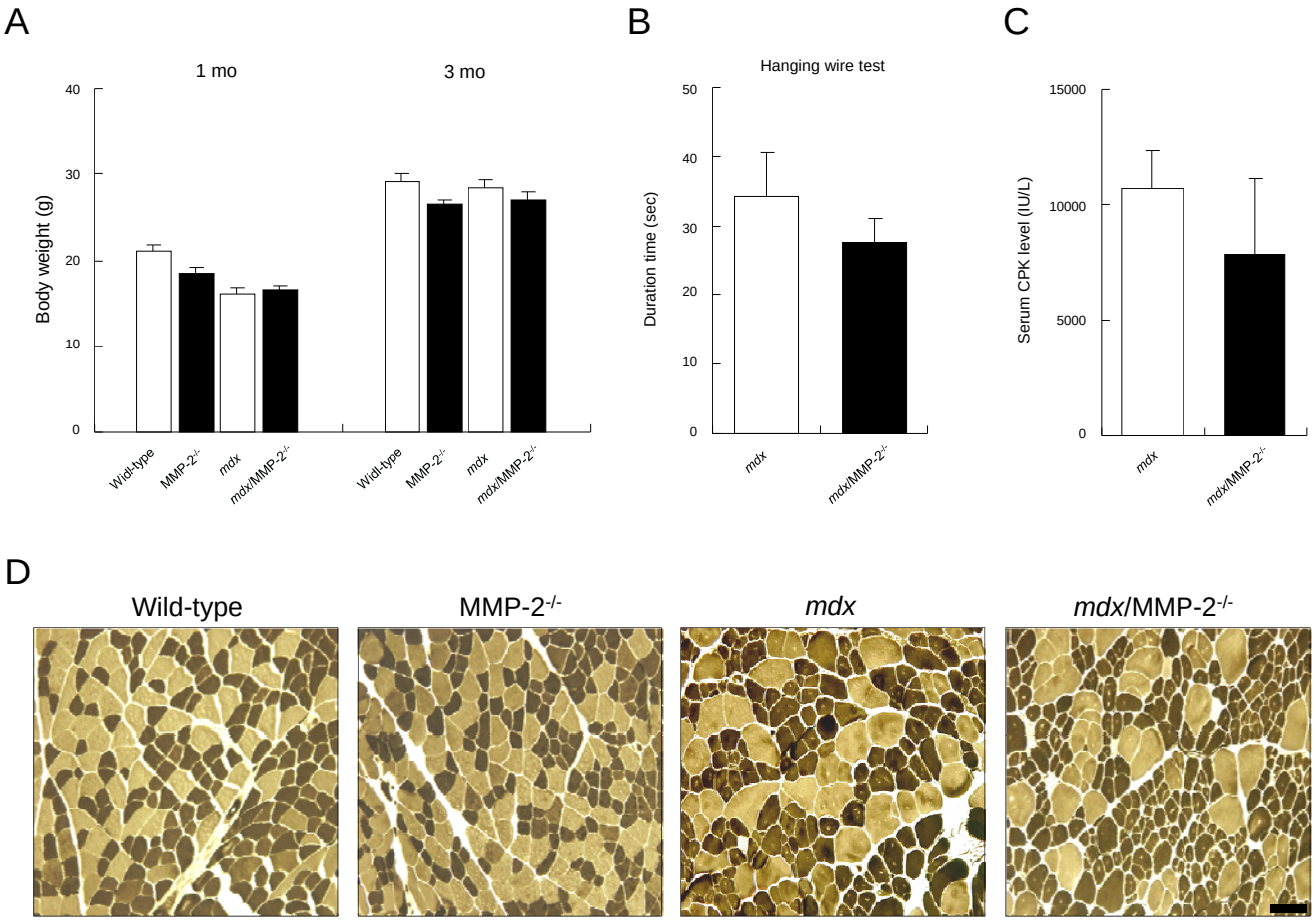

Supplemental Figure 3

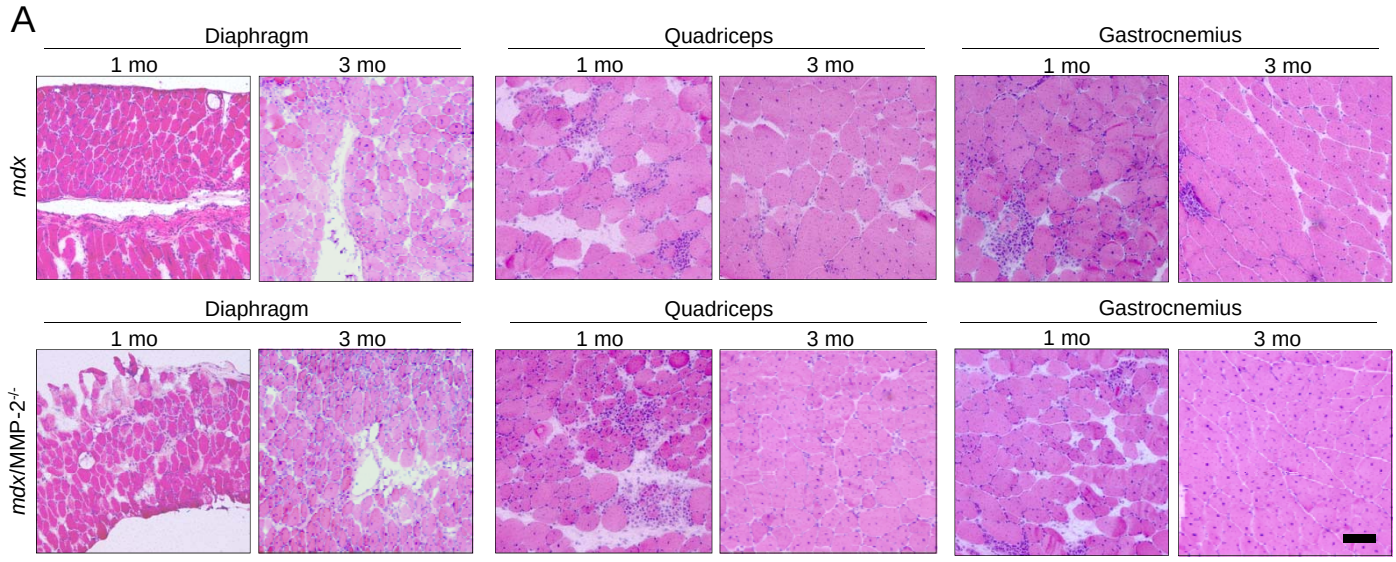

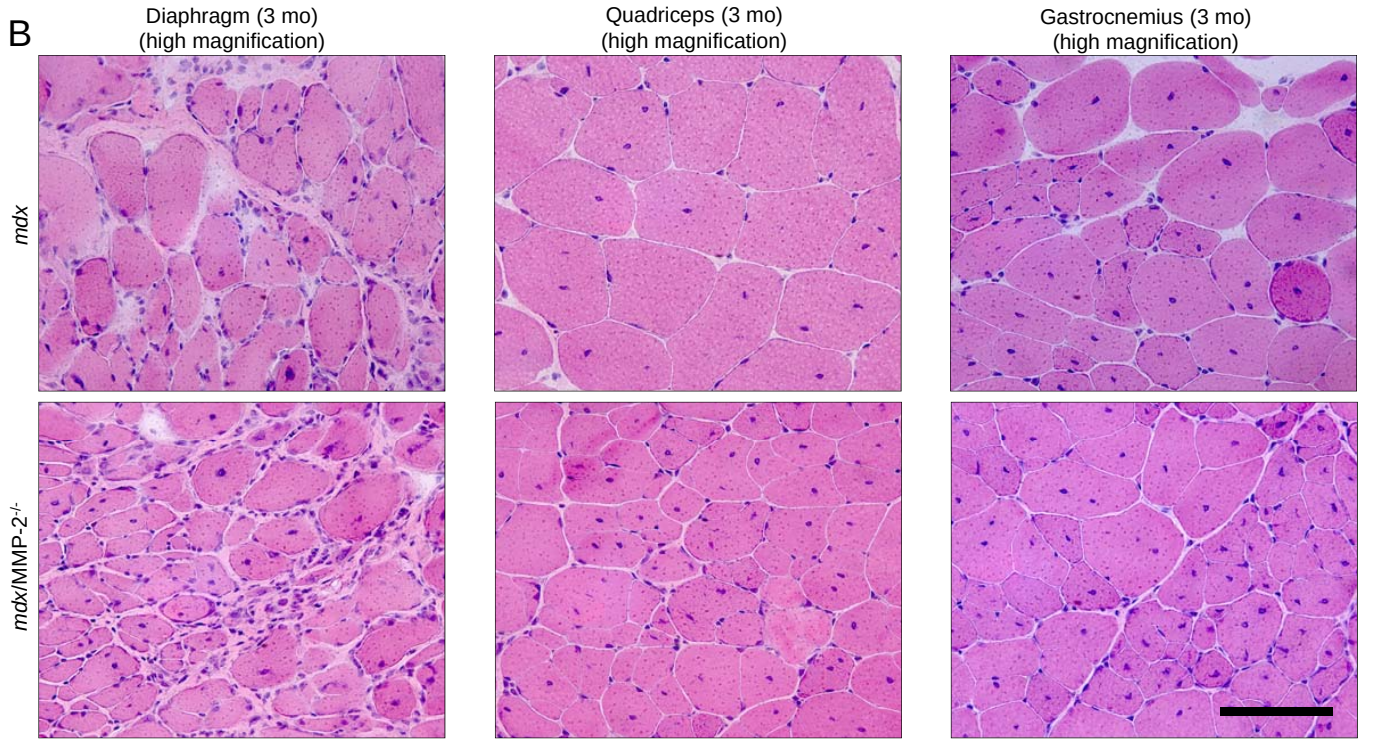

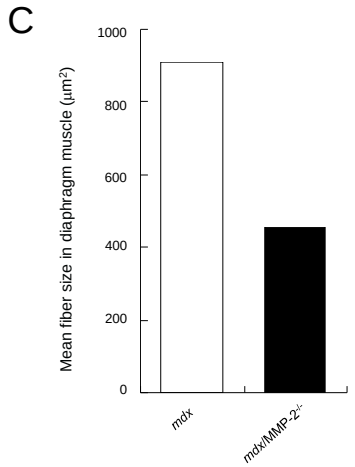

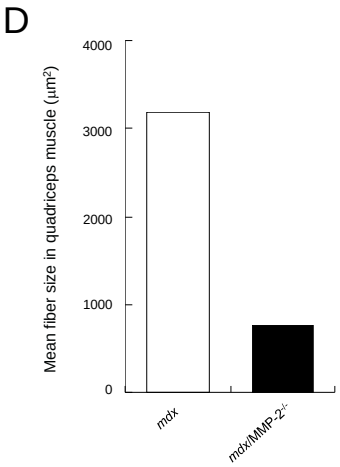

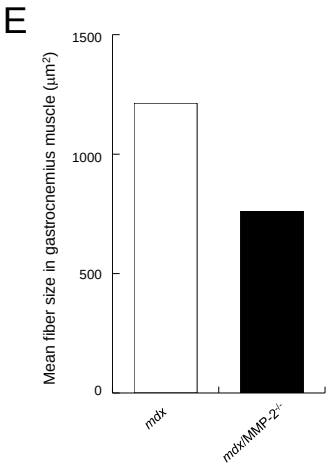

Supplemental Figure 4

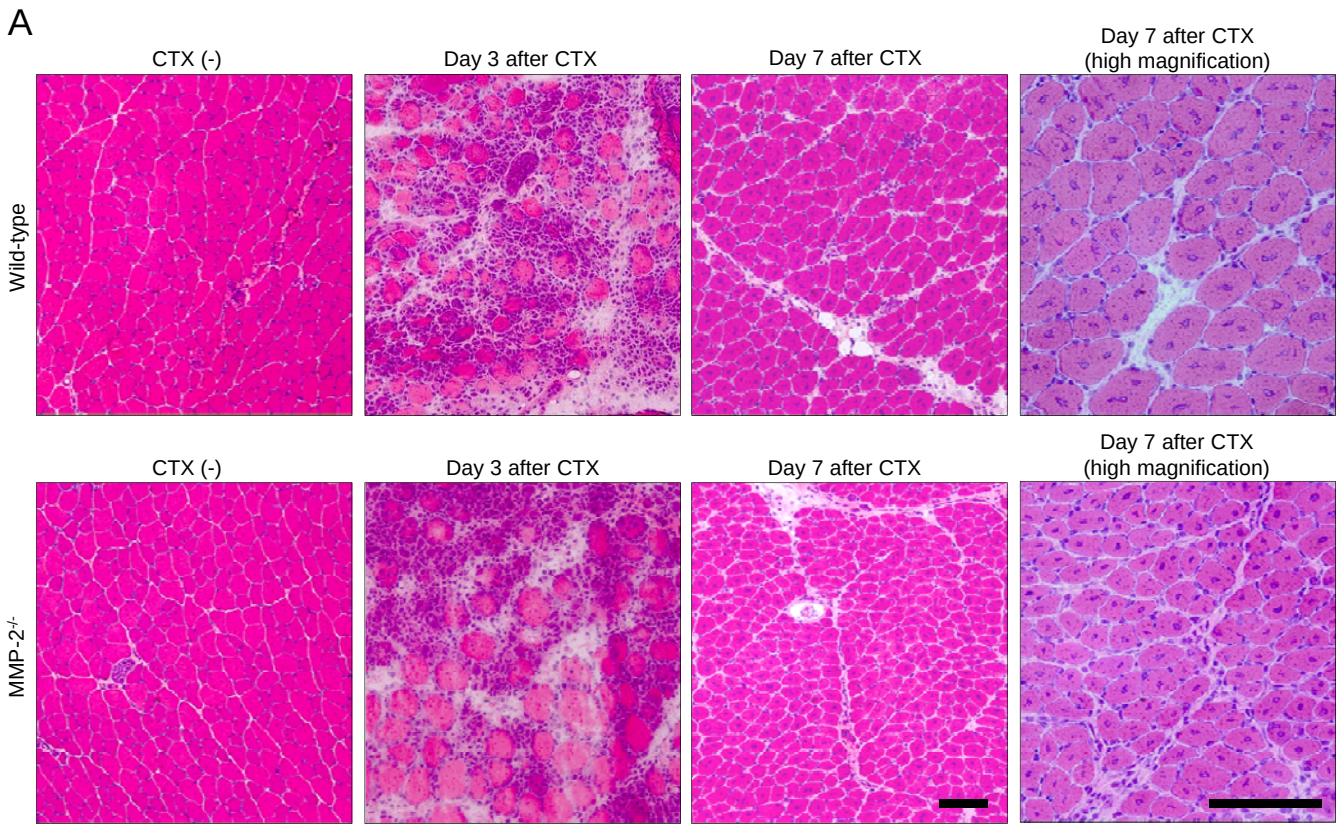

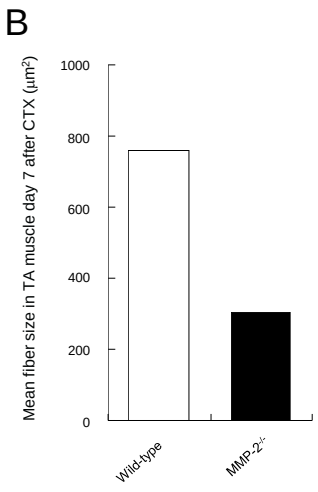

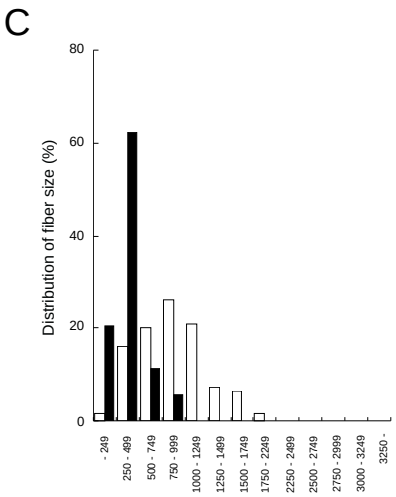

Supplemental Figure 5

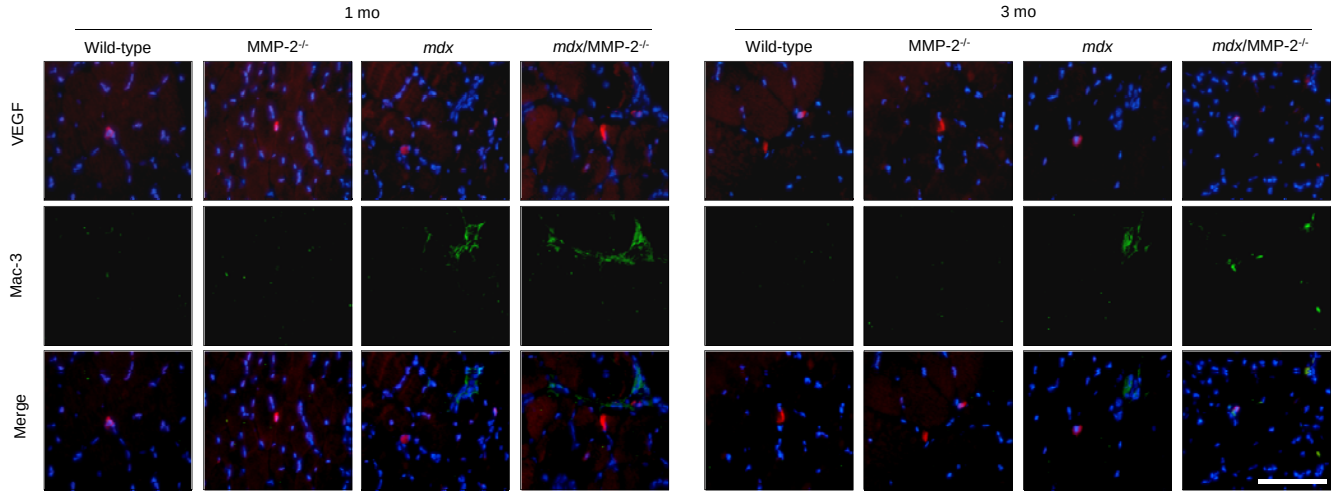

Supplemental Figure 6

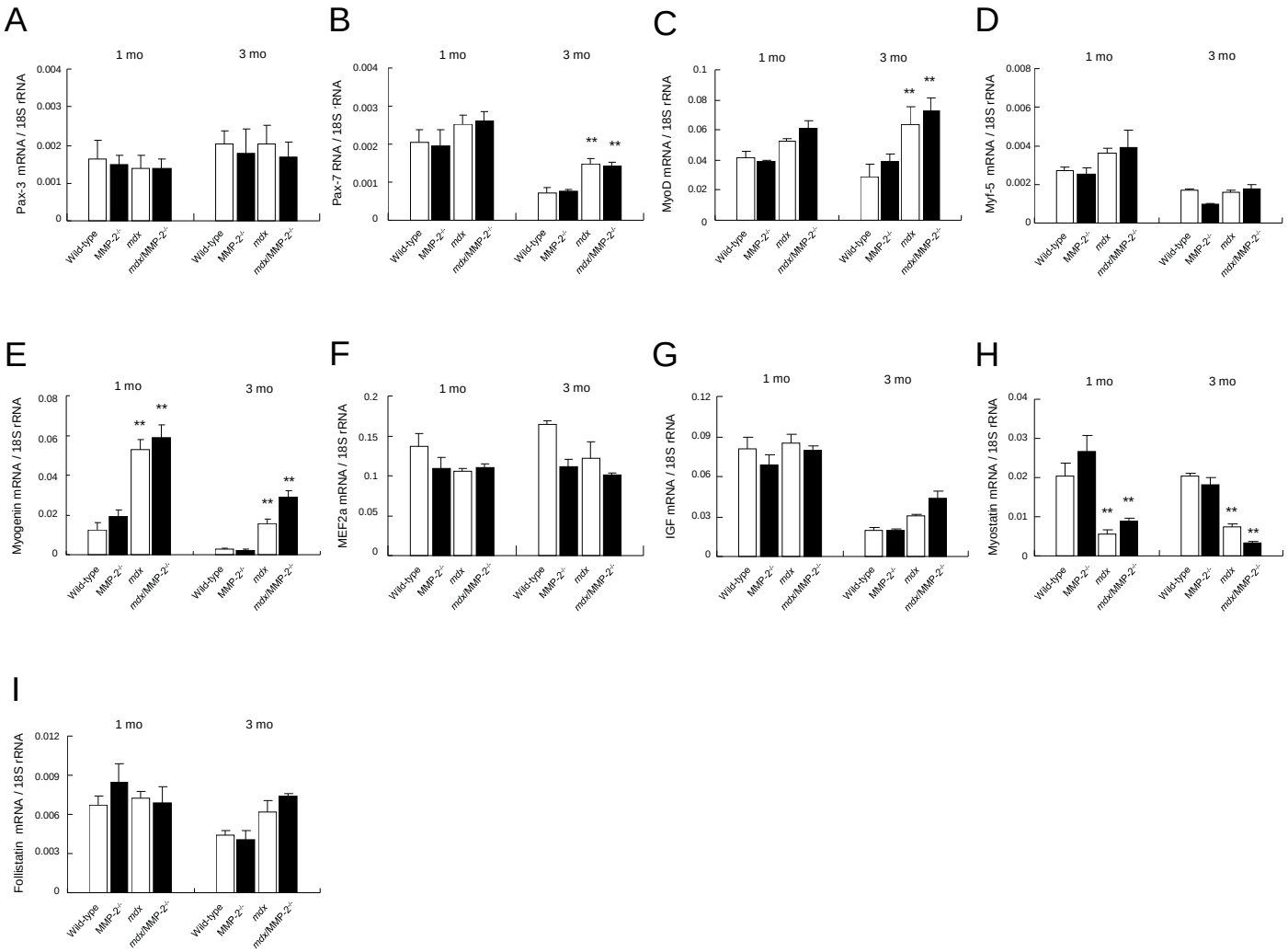

Supplemental Figure 7